SHRIMP U-Pb zircon dating of Archean core complex formatio and pancratonic strike-slip deformation in the East Pilbara Granite-Greenstone Terrain

Zegers, T.E.; Nelson, D.R.; Wijbrans, J.R.; White, S.H.

published in
Tectonics
2001

DOI (link to publisher)
10.1029/2000TC001210

document version
Publisher's PDF, also known as Version of record

TECTONICS, VOL. 20, NO. 6, PAGES 883-908, DECEMBER 2001

SHRIMP U-Pb zircon dating of Archean core complex formation and pancratonic strike-slip deformation in the East Pilbara Granite-Greenstone Terrain

T.E. Zegers,[1] D.R. Nelson,[2,3] J.R. Wijbrans,[4] and S.H. White[1]

Abstract. Sensitive high-resolution ion microprobe (SHRIMP) U-Pb dating of zircons from granitic rocks in the East Pilbara Granite-Greenstone Terrain has provided time constraints for main tectonic events in the Shaw Granitoid Complex and has shown that deformation was intricately related to granitoid intrusion. The earliest recognized deformation activity occurred within the Split Rock Shear Zone (SRSZ), probably between 3470 and 3420 Ma. The timing, geometry, and kinematics of this shear zone suggest that it was a midcrustal detachment in a core complex type extensional setting. It was active during the intrusion of synkinematic sheeted granodiorite of the North Shaw Suite and brittle extensional faulting within the upper crust. Samples of gray migmatic gneiss and a diorite that occur structurally below the SRSZ were dated at 3451±1 Ma and 3463±2 Ma, respectively, indicating that melting and metamorphism took place in the lower units during extension in the middle to upper crust. The 3470-3420 Ma extensional event is most consistent with extensional collapse, possibly as a result of delamination or convectional thinning of part of the lithosphere. Activity on the pancratonic strike-slip Mulgandinnah Shear Zone (MSZ) was constrained by the crystallization age of a synkinematic granitic dyke to have occurred at 2934±2 Ma. The MSZ and activity on the Sholl Shear Zone of the western Pilbara at 2960 Ma [*Smith et al.*, 1998] are consistent with a regional NW-SE directed compressional stress field at this time. Steepening of greenstone belt stratigraphy has been attributed to diapirism, but probably occurred after a 3300-3200 Ma compressional event and following deposition of the youngest clastic sediments in the eastern Pilbara stratigraphic sequence. Diapiric processes did not play a major role during the early evolution of the eastern Pilbara Craton from 3470 to 3300 Ma.

[1]Vening Meinesz Research School of Geodynamics, Faculty of Earth Sciences, Utrecht University, Utrecht, Netherlands.

[2]Geological Survey of Western Australia, East Perth, Australia.

[3]Also at Western Australian Isotope Studies Research Group, Department of Applied Physics, Curtin University of Technology, Perth, Australia.

[4]Department of Isotope Geochemistry, Faculty of Earth Sciences, Vrije University, Amsterdam, Netherlands.

Paper number 2000TC001210.
0278-7407/01/2000TC001210$12.00

1. Introduction

In the last 10 years, plate tectonic concepts based on the study of the modern Earth have been applied to the interpretation of Archean granite-greenstone terrains. Late Archean terrains, such as those that comprise much of the Superior Province of North America, have been interpreted as resulting from the lateral accretion of island arcs and oceanic plateaus [e.g., *Polat et al.*, 1998; *Puchel et al.*, 1998], analogous to the formation of Phanerozoic collision belts. However, processes common in Phanerozoic terrains are not easily recognized in mid-Archean granite-greenstone terrains, and so processes responsible for the formation of granite-greenstone terrains such as those of the Pilbara and Kaapvaal Cratons remain enigmatic. *De Ronde and de Wit* [1994] interpreted the tectonic evolution of the Barberton Belt of the Kaapvaal Craton in terms of modern-day tectonic processes, as terrains formed in oceanic and island arc environments. *Barley* [1993] interpreted the geochemistry of volcanic rocks in the Pilbara greenstones in terms of volcanic arcs. In contrast, *Choukroune et al.* [1995] and *Collins et al.* [1998] argued that the Pilbara granite-greenstone terrain was formed by processes unique to the Archean, with deformation having resulted from solid-state diapirism.

Controversy over the tectonic processes responsible for the formation of mid-Archean granite-greenstone terrains is in part due to a paucity of detailed structural and geochronological investigations. Geometrical and kinematic relationships within and between the greenstone and granitoid components of these terrains are generally poorly understood.

Here we report the results of the sensitive high-resolution ion microprobe (SHRIMP) U-Pb zircon dating of granitic rocks from the Shaw Granitoid Complex (SGC) of the East Pilbara Granite-Greenstone Terrain. Sampling for geochronology was undertaken following detailed field and structural investigations, and with the aim of elucidating the nature of the tectonic processes involved in the formation of a well-preserved mid-Archean granite-greenstone terrain. The results of this study are combined with previously published dates and observations from the area, in order to critically assess the contrasting tectonic models for the development of the Pilbara granite-greenstone terrain.

In particular, the hypothesis that the early evolution of the Shaw Granitoid Complex involved core complex style extension coeval with tonalite-trondhjemite-granodiorite(TTG) magmatism is evaluated, and the timing and role of diapirism and pancratonic strike-slip shear zones are assessed.

2. Geological Background

The Pilbara Craton is broadly divisible into an older granite-greenstone terrain, formed between about 3.6 and 2.8 Ga, and a younger cover sequence that includes the volcanic and clastic

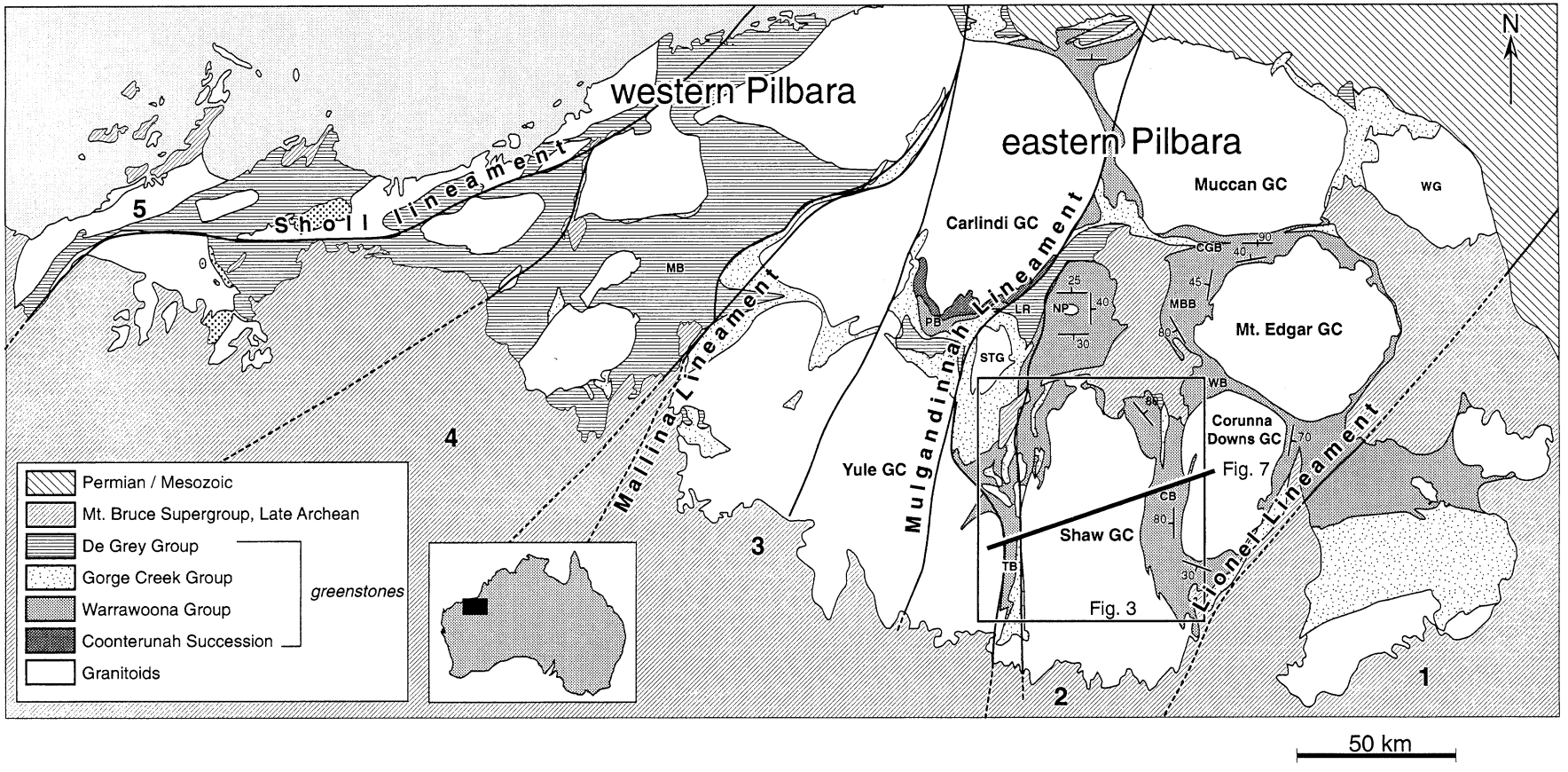

Figure 1. Map of the Pilbara granite-greenstone terrain. The location of the study area in Australia is shown in the black rectangle in the inset. Lineaments are redrawn after *Krapez and Barley* [1987]. The western Pilbara corresponds to domain 4 and 5, and the eastern Pilbara corresponds to domain 1 to 3. MB, Mallina Basin; LR, Lalla Rookh Basin; STG, Strelley Granitoid Complex; NP, North Pole dome; WG, Warrawagine Granitoid Complex; CB, Coongan Belt; WB, Warrawoona Belt; CGB, Coppin Gap Belt; PB, Pilgangoora Belt.

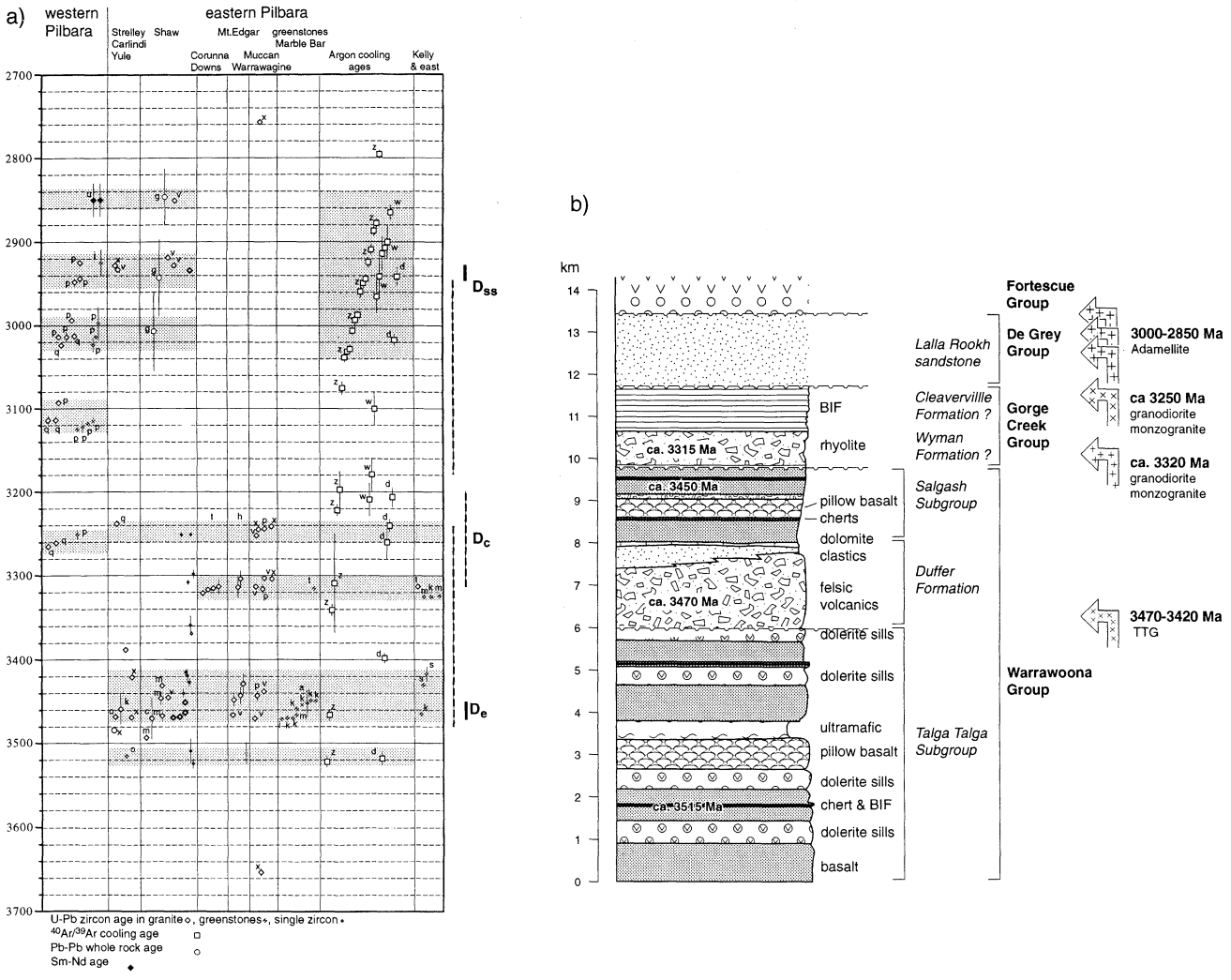

Figure 2. a) Published U-Pb, Pb-Pb, and $^{40}Ar/^{39}Ar$ ages in the Pilbara granite greenstone terrain shown on a time line. Error bars are indicated (1 σ). References are from a, *Pidgeon* [1978a]; b, *Pidgeon* [1978b]; c, *Williams et al.* [1983]; d, *Davids et al.* [1997]; e, *Bickle et al.* [1983]; g, *Bickle et al.* [1989]; k, *Thorpe et al,* [1992]; m, *McNaughton et al.* [1993]; o, *Buick et al.* [1995]; p, *Nelson* [1996]; q, *Smith et al.* [1998]; s, *Barley et al.* [1998]; t, *Barley and Pickard* [1999]; v, *Nelson* [1997a]; w, *Wijbrans and McDougall* [1987]; x, *Nelson* [1999]; z, *Zegers et al.* [1999]. Large symbols indicate various dating methods; small symbols represent single zircon U-Pb ages, both xenocrystic and recrystallized parts of zircons. The shaded bars indicate periods of major rock-forming events in the east and west Pilbara. Note that rock-forming events in the western Pilbara are different than in the eastern Pilbara but are consistent to a large extent within the eastern Pilbara. Stippled lines on the right-hand side indicate time control to the three main deformation events in the Shaw area (D_e, extension, D_c, compression, D_{ss}, strike-slip deformation) prior to this study; solid lines indicate time control with SHRIMP U-Pb ages reported here. (b) Simplified stratigraphy of the Coongan Belt with events of granite intrusion in the eastern Pilbara.

sedimentary rocks and thick-banded iron formations of the < 2.8 Ga Mount Bruce Supergroup (Figure 1). The 60,000 km² granite-greenstone component of the Pilbara Craton may be subdivided into western and eastern granite-greenstone domains (Figure 1). The latter contains the oldest components, which range in age between 3.6 and 2.8 Ga. The western domain contains components with ages between 3.3 and 2.9 Ga and has been interpreted, on the basis of geochronology (see Figure 2), as a separate terrane that was accreted to an older east Pilbara continental nucleus [*Smith et al.*, 1998].

The granite-greenstone component of the Pilbara Craton is transected by NE trending pancratonic shear zones [*Zegers et al.*, 1998; *Smith et al.*, 1998; *van Kranendonk and Collins,* 1998] that have been interpreted by some authors [e.g., *Krapez and Barley,* 1987] as tectonostratigraphic terrane boundaries dividing the granite-greenstone terrain into five terranes (see Figure 1). This study concentrates on the area of the Shaw Granitoid Complex in which detailed structural and kinematic mapping has been carried out [*Zegers et al.,* 1996, 1998]. Previous lithological mapping, stratigraphic and geochronological studies in the

eastern Pilbara region have shown that although lateral variations in stratigraphy exist and the geometry is complicated by locally intense deformation and alteration, the eastern part of the Pilbara Craton was formed during a number of magmatic events at circa 3650 Ma, 3515 Ma, 3470-3420 Ma (TTG), 3320 Ma, 3250 Ma, and 3000-2850 Ma (Figure 2).

The oldest dated rock (3655±6 Ma) identified so far within the Pilbara granite-greenstone terrain is a banded orthogneiss from the Warrawagine Granitoid Complex [*Nelson,* 1999] in the NE part of the granite-greenstone terrain (Figure1). *Thorpe et al.* [1992] have reported an even older xenocrystic zircon at 3724 ±1 Ma.

The 3515-2950 Ma volcano-sedimentary supracrustal rocks in the eastern Pilbara Craton may be subdivided into four sequences (Figures 1 and 2) that are separated by unconformities: the Coonterunah Group and the Warrawoona, Gorge Creek and De Grey Groups. The Coonterunah Group has only been described in the Pilgangoora Belt (Figure 1), whereas the other three have been recognized throughout the eastern Pilbara. The lithologies of the supracrustal rocks range from almost entirely volcanic (mafic–ultramafic, minor felsic volcanic and banded iron formation–chert) at the base, to clastic sediment dominated in the uppermost units. The intrusive rocks consist of 3470-3417 Ma tonalite-trondhjemite-granitoid suites, circa 3320 and 3250 Ma granodiorites to monzogranites and 3000-2850 Ma monzogranites (see Figure 2 for summary). Granitoid complexes typically consist of rocks from a number of different magmatic episodes. The Shaw Granitoid Complex contains 3470-3417 Ma and 3000-2850 Ma components.

The earliest tectonic phase recognized in the Shaw area is extensional (D_e) with ENE transport in a core complex type geometry during deposition of the Warrawoona Group [*Zegers et al.,* 1996]. D_e resulted in synsedimentary growth faults, and a detachment shear zone at the contact between the granitoid bodies and adjacent greenstones has been recognized. A subsequent major deformational phase, recognized in the Shaw area, is an E-W compressional phase (D_c) during deposition of the Gorge Creek Group, which resulted in folding and low-angle thrusting of the volcano-sedimentary stratigraphy [*Boulter et al.,* 1987; *Zegers,* 1996]. In a later phase of localized deformation (D_{ss}), pancratonic strike-slip shear zones were active [*van Kranendonk and Collins,* 1998; *Zegers et al.,* 1998].

For the timing of deformation, $^{40}Ar/^{39}Ar$ dating has proven to be especially powerful in the greenstone belts, where the rocks are more likely to contain amphiboles, and the heat effects of late to posttectonic granite intrusions are limited [*Zegers et al.,* 1999]. $^{40}Ar/^{39}Ar$ cooling ages, mainly of hornblende (Figures 2 and 3), have so far provided the only age information for the structural events from the Shaw area. $^{40}Ar/^{39}Ar$ cooling ages of syntectonic and posttectonic amphiboles from shear zones have provided minimum constraints for the time of activity (see Figure 2 for an overview). *Zegers et al.* [1999] showed that the Split Rock Shear Zone predated 3222±13 Ma, the oldest cooling age from the mylonite. The $^{40}Ar/^{39}Ar$ cooling ages have constrained the compressional event (D_c) to pre-3197±44 Ma, and D_e structures deform Wyman felsic volcanics deposited at circa 3325 Ma.

The timing of amphibolite grade deformation (D_{ss}) in the craton scale strike-slip Mulgandinnah Shear Zone (MSZ) is pre-2944±9 Ma, as indicated by the oldest hornblende cooling age obtained from a MSZ mylonite [*Zegers et al.,* 1999]. In this study, SHRIMP U-Pb zircon dates have been obtained for samples from the Shaw Granitoid Complex in order to constrain the time of activity of major shear zones that formed during D_e (the Split Rock Shear Zone) and D_{ss} (the Mulgandinnah Shear zone).

3. Samples

3.1. Structural Context of Samples

Major structures and the main lithological components of the Shaw Granitoid Complex, as well as sampling locations from this study and previously published geochronology, are shown in Figure 3. The central part of the Shaw Granitoid Complex consists of migmatic gray gneisses and diorites (Figure 4a) which have been variably deformed, under upper amphibolite to granulite facies conditions, into decimeter-scale folds and associated crenulation cleavage (Figure 4b). Enclaves in the migmatitic gneisses include amphibolite-grade metabasaltic and metasedimentary rocks [*Bickle et al.,* 1985] in the western SGC.

The gray gneisses are truncated to the east and north by the Split Rock Shear Zone (SRSZ), an ~2 km wide amphibolite-grade mylonite zone (Figures 4c and 4d), which forms part of a dome shape with a consistently ENE plunging lineation. The sense of shear is (north) east up [*Zegers et al.,* 1996, 1998]. The SRSZ can be traced from the southeast to the north, changing strike from north to west. The southwest trending part of the SRSZ closest to the MSZ is obscured by younger granites and poor exposure, but its continuation has been inferred as the boundary between migmatic gneisses and the outer North Shaw Suite [*Bickle et al.,* 1989]. The North Shaw Suite forms the northern and eastern margins of the Shaw Granitoid Complex and has been dated in the northwestern part of the SGC complex (Figure 3) at 3467±6 Ma [*McNaughton et al.,* 1993].

In the northwestern part of the Coongan belt, listric extensional faults, active during deposition of the 3470-3450 Ma Duffer Formation, sole into the greenschist facies Shark Gully Shear Zone (SGSZ, Figure 3). To the south the SGSZ merges with amphibolite facies mylonites of the SRSZ at the granite-greenstone contact (Figure 4e) (cf. see *Zegers et al.* [1996] for a detailed discussion). The SRSZ has the same direction of transport as the SGSZ and the brittle extensional faults, and the geometry of the combined brittle and ductile structures closely resembles that of a core complex. *Zegers et al.* [1996] argued that the SRSZ is a basal midcrustal detachment to the upper crustal extensional faults in a core complex type setting. To test this hypothesis, the cooling histories of the hanging wall and footwall were examined by $^{40}Ar/^{39}Ar$ dating (*Zegers et al.,* 1999). Unfortunately, the argon systematics do not record the thermal events, probably as a result of resetting by later intrusion events.

In the southeast, where the SRSZ and the SGSZ merge, the mylonitic foliation of the SRSZ has been intruded by sheets of granodiorite, which, on lithological and geochemical grounds, are inferred to belong to the North Shaw Suite. Dual relationships between the shear zone fabric of the SRSZ and the granodiorite were found. Close to the contact with the gray gneisses the granodiorite has been deformed and shows an intense SRSZ mylonitic fabric. Close to the greenstones, the granodiorite contains a weak SRSZ protomylonitic fabric (Figure 4f) is intrusive in mylonitic greenstones and contains mylonitic amphibolite enclaves (Figure 4g). These relationships suggest that the SRSZ was active during intrusion of sheeted granodiorite of the North Shaw Suite.

The western part of the Shaw Granitoid Complex has been truncated by the sinistral Mulgandinnah Shear Zone, which is part of a lineament (Figure 1) that extends northward into the Pilbara Craton (see *Zegers et al.* [1998] for a detailed

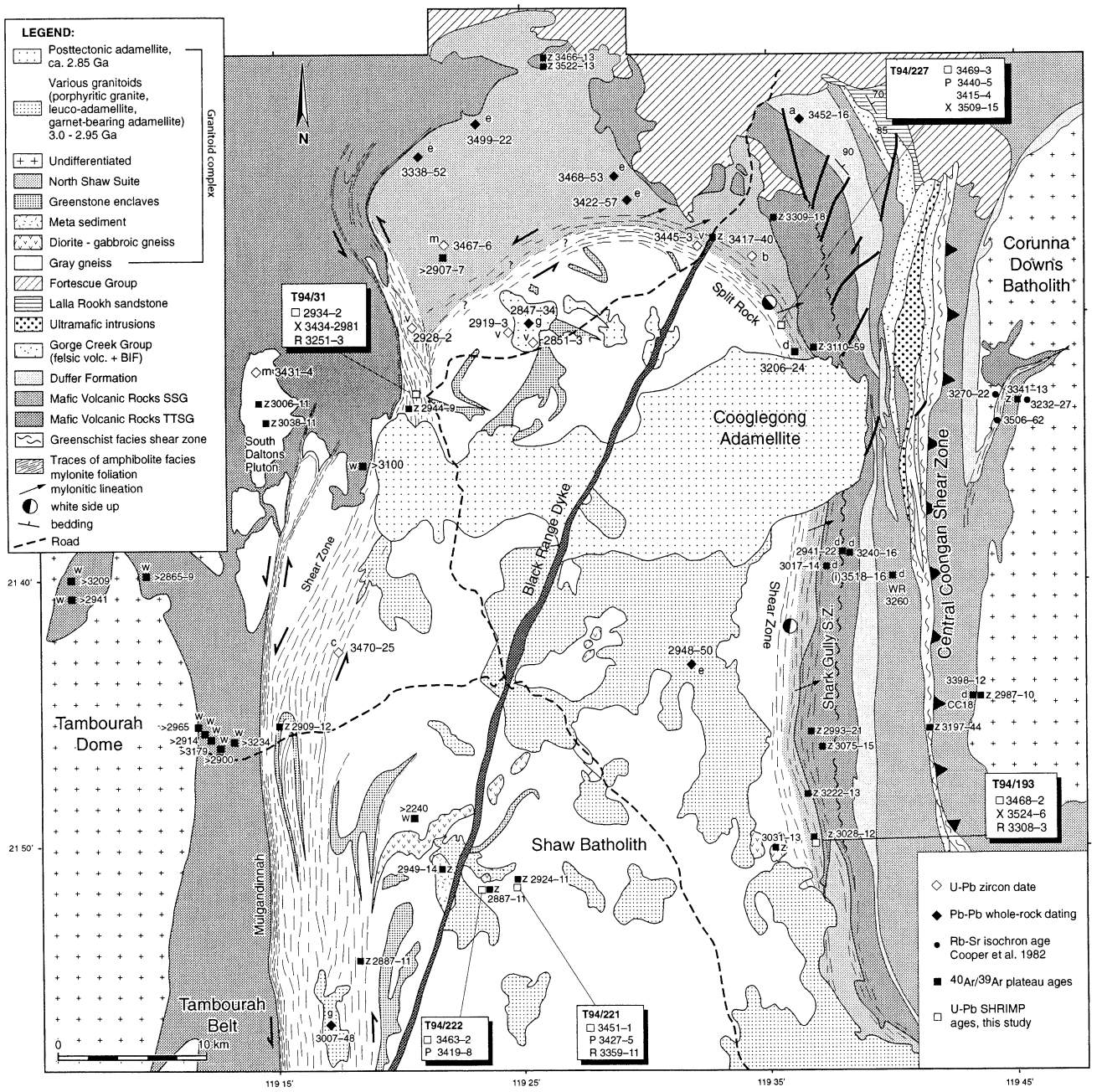

Figure 3. The Shaw Area, showing the major structures (the Split Rock Shear Zone, the Shark Gully Shear zone, the Central Coongan Shear Zone, and the Mulgandinnah Shear Zone). For references to previously published ages, see caption of Figure 2. *X*, xenocrystic age; *R*, recrystallized (part of) zircon; *P*, other pooled age group.

discussion). The MSZ truncates the gray gneisses and the North Shaw Suite, but it has been intruded and is truncated by the circa 2850 Ma [*Nelson,* 1998] Cooglegong Adamellite. Syntectonic granitic dykes intrude into the ultramylonitic fabric of the MSZ and show the same mylonitic folation and lineation as the ultramylonites (Figure 4h).

The samples selected for U-Pb zircon geochronology in this study were chosen specifically to determine the age of gray gneisses and diorites, to determine whether they are pre-Warrawoona basement, and to provide age constraints for the activity of the SRSZ and MSZ. Sample localities and lithological characteristics are summarized in Table 1.

3.2. Sample Description

3.2.1 Gneisses from the central part of the Shaw Granitoid Complex. Reliable age data were not available for the migmatic gray gneiss and dioritic components of the Shaw Granitoid Complex. A SHRIMP U-Pb date of 3470±25 Ma obtained by Williams et al. [1983] (see Figure 3) on a sample of gray gneiss is

from a site within the MSZ, and it is uncertain whether this is from the same gray gneisses that from the central part of the Shaw Granitoid Complex. Two samples were collected from the central part of the Shaw Granitoid Complex, some distance from the SRSZ and the MSZ, in order to determine their ages and to resolve the timing relationships between these components.

Sample T94/221 was collected from a large outcrop of fresh gray gneiss within the bed of the Shaw River. This locality consists mainly of homogeneous, fine-grained biotite granodiorite gneiss with nebulitic compositional banding and minor (10 cm thick) bands of quartz diorite. The banding, which is locally folded with a fold axis plunging moderately (20°-40°) to 330°, is generally NNE trending, and dips toward the east at 30°-40°. Original intrusive relationships between the gray gneiss and dioritic bands could not be established. A mineral lineation, formed by aligned biotite aggregates and hornblende grains on the foliation parallel to the banding, is parallel to the fold axis. Sample T94/221 is of homogeneous biotite granodiorite that has been completely recrystallized to a granoblastic assemblage of plagioclase, minor K-feldspar, quartz, biotite, accessory titanite, epidote and opaques. A diorite sample, T94/222, was collected from an ~50 x 20 m outcrop located ~1 km west of the site of T94/221. The outcrop consists entirely of coarse-grained, foliated quartz diorite. The tectonic foliation is WSW trending and steeply west dipping, with a weakly developed mineral lineation plunging 40° to the south. The diorite consists of plagioclase, clinopyroxene, hornblende, and quartz, with accessory titanite and zircon, and has been recrystallized to a granoblastic texture.

3.2.2. Split Rock Shear Zone. Two samples were collected in order to constrain the timing of movement along the SRSZ. Sample T94/193 is of a biotite–hornblende granodiorite from a well-exposed area ~300 m from the granitoid-greenstone contact. On lithological grounds this granodiorite is inferred to be part of the 3468 Ma [McNaughton et al., 1993] North Shaw Suite. The contact is complicated by contact-parallel intrusion of garnet-bearing granites and a complex network of pegmatites. The biotite-hornblende granodiorite crops out in a linear zone between the basal SRSZ and the greenstones. It is weakly foliated and lineated parallel to the SRSZ close to the contact with the greenstones, with the strain intensity increasing toward the basal SRSZ. The granodiorite can be seen to have intruded the greenstones, with foliated amphibolite enclaves in the granodiorite close to the contact (Figure 4g). Sample T94/193 was taken from an outcrop showing a proto-mylonitic foliation (Figure 4f) and downdip lineation. The sample contains plagioclase, K-feldspar, quartz, biotite, green hornblende and accessory titanite and epidote. Quartz grains show undulose extinction and subgrain formation.

Sample T94/227 was collected from an outcrop in a river bed in the central part of the basal SRSZ. It shows a strong mylonitic foliation (Figures 4c and 4d) and a strong stretching lineation, with asymmetric clasts indicating an east up sense of shear. The sample shows compositional layering parallel to the foliation of granodiorite and pegmatite bands, all equally deformed. The compositional layering suggests that there are several igneous phases present, but deformation has obscured any original intrusive relations. The mylonite forms the contact between the North Shaw Suite granodiorite and the migmatic gneisses (Figure 3). It is not clear whether the sampled mylonite was originally part of the gneiss or of the granodiorite. It contains K-feldspar, plagioclase, quartz, biotite partly altered to chlorite, garnet in pegmatite layers, minor epidote and opaques. On a microscale the fabric is mylonitic, with quartz ribbons and asymmetric clasts in a fine-grained, dynamically recrystallized matrix.

In summary, sample T94/193 is of a granodiorite that has intruded the SRSZ amphibolite facies mylonitic foliation in the greenstones, whereas the mylonitic granitoid rock sample T94/227 is from a high strain part of the basal SRSZ. These two samples will therefore provide minimum (T94/193) and maximum (T94/227) age constraints for deformation along the SRSZ, provided that the amphibolite facies mylonitic foliation in both granitoids and greenstones are part of one shear zone system.

3.2.3. Mulgandinnah Shear Zone. The MSZ consists of amphibolite facies mylonitic and ultramylonitic rocks of mainly granitic composition with amphibolitic enclaves. Several generations of pegmatites are present in the MSZ and the ultramylonite zones have been intruded by granitic dykes during deformation. The time of crystallization of some of these dykes may constrain the time for movement of the MSZ. One of these dykes was sampled (T94/31) from a large outcrop in the Shaw River (Figure 4h). The dyke is ~2 m wide and cuts across the ultramylonitic foliation at a low angle, but it also shows the same ultramylonitic foliation and lineation, indicating that it intruded during formation of the ultramylonitic foliation.

The granitic dyke contains K-feldspar, plagioclase, quartz, biotite partly altered to chlorite, and epidote. The sample shows a mylonitic microstructure with quartz ribbons, asymmetric clasts, and reduced grain size of the matrix.

4. Results of SHRIMP U-Pb Zircon Analyses

All samples contained sufficient zircons to enable ~50 grains >100 μm to be prepared for analysis. Table 1 provides a summary of the characteristics of the zircon populations for each sample. Cathodoluminescence images of some typical zircon

Figure 4. (a) Dioritic band (D) in gray migmatitic gneiss, representative of sample T94/222. (b) Folded gray gneiss with leucosomes (L) following the crenulation foliation planes. Representative of sample T94/221. (c) Mylonitic foliation of the Split Rock Shear Zone forming the boundary between the gray gneisses to the west and the North Shaw Suite to the east. (d) Mylonitic fabric of the SRSZ, approximately parallel to the ENE pitching stretching lineation. The plagioclase σ clasts (cl) and S-C fabric (s-c) indicate an east up sense of shear. The lens cap has a diameter of 5 cm. Sample T94/227 is of this mylonitic granitic rock. (e) Mylonitic S-C fabric in amphibolite grade greenstones (subhorizontal view) at the southern contact between the Coongan Belt and the Shaw Granitoid Complex. The S-C fabric indicates an east up sense of shear. The diameter of the coin is 2 cm. (f) Protomylonitic foliation in the North Shaw Suite with locally a more intense mylonitic fabric (m). This intensity of deformation is typical for the North Shaw Suite closer to the greenstones, away from the contact with the gray gneiss. Sample T94/193 is of the protomylonitic part of the North Shaw Suite. (g) Intrusive relationship between granodiorite, probably the North Shaw Suite (nss) and mylonitic amphibolite enclaves (am). (h) Granitic dyke (D) intruding the ultramylonitic foliation of the Mulgandinah Shear Zone at a small angle. The granitic dyke shows the same foliation/lineation as the ultramylonite, indicating intrusion during deformation. Sample T94/31 is of the granitic dyke.

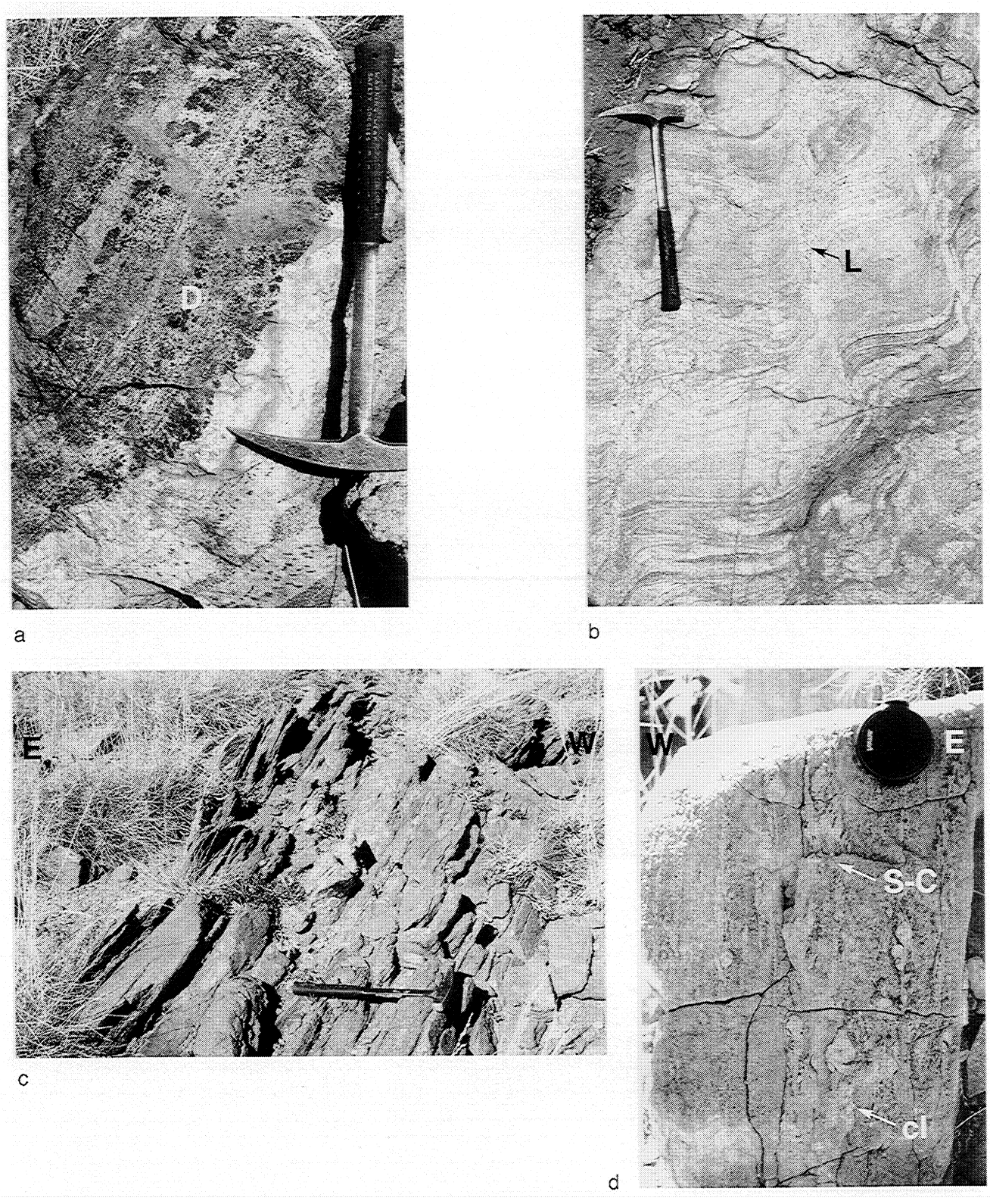

Figure 4.

microstructures are given in Figure 5. Analytical procedures and results are summarized in Appendix A and Table 2, respectively. All errors cited in the text are at the 95% confidence level unless otherwise indicated; errors on individual analyses given in tables 1 and 2 are at the ±1 σ level.

4.1. Sample T94/31 Syn-Mulgandinnah Shear Zone Granite

This sample contained short prismatic, planar zoned, light brown zircons, many with rounded, irregular, or planar zoned

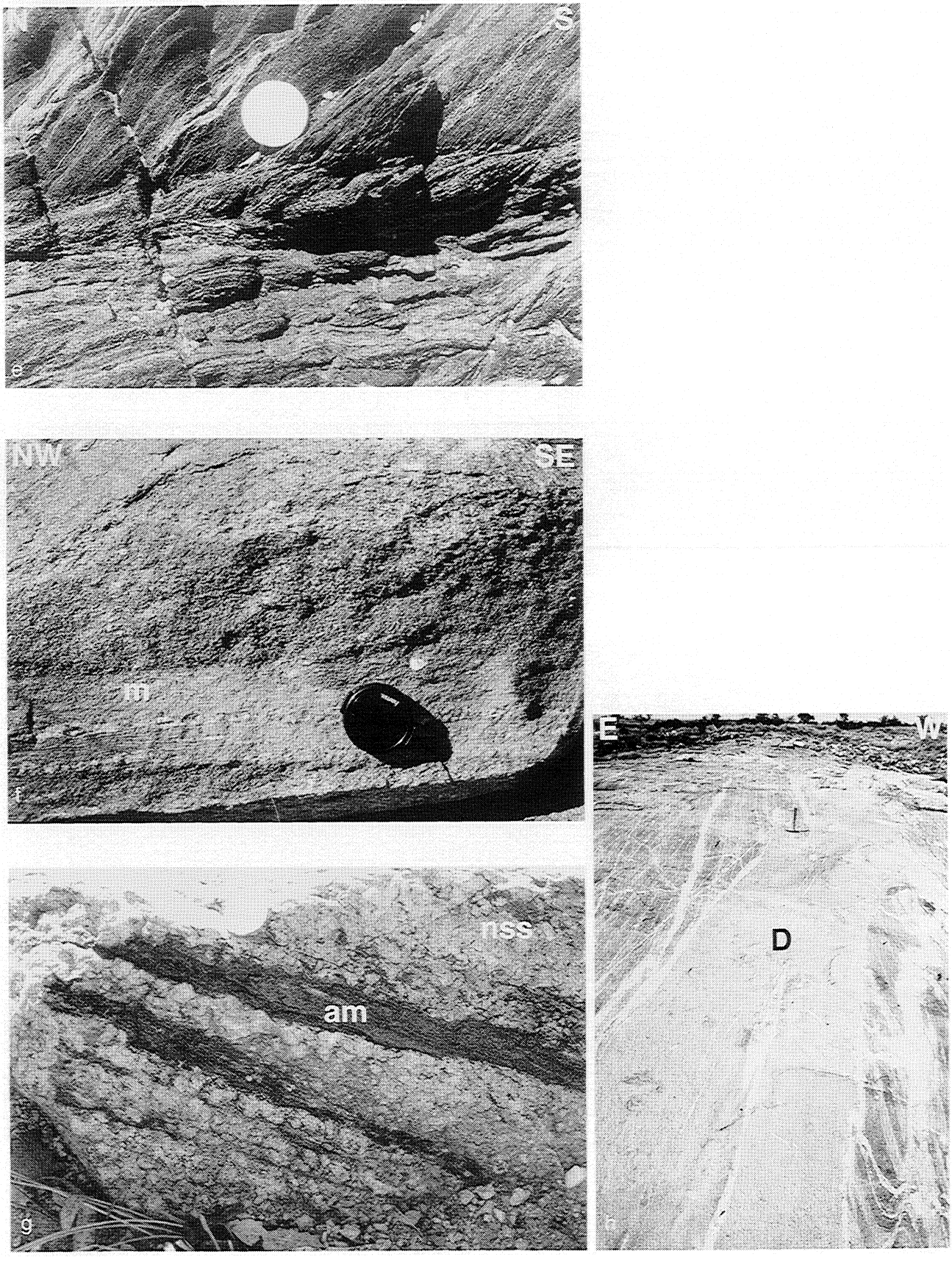

Figure 4. (continued)

Table 1. U-Pb Sample Location Coordinates, Sample Characteristics, Zircon Characteristics, and Summarized Results of U-Pb SHRIMP Dating[a]

Sample	Coordinates	Sample Characteristics	Structural Implication	Zircon Characteristics				Crystallization Age		Xenocrystic Zircons		Two-Spot Zircons	
				Shape	Length/ Width	Cores	Texture	Other Pooled Ages		New Growth or Recrystallization		Core	Rim
T94/31	742.0E, 7616.0S	biotite granite dike with a mylonitic foliation/lineation	intrudes during deformation in the MSZC	short prismatic slightly rounded	3.7-1.8	featureless and recrystallized cores 20%	irregular planar zoning	2934±2		3434-2981	3251±3	2909±5	2937±7
												3434±5	3369±3
T94/193	768.5E, 7583.6S	medium-grained biotite granodiorite, weakly foliated	intrusion partly postdates SRSZ fabric	short prismatic	3.9-2.4	featureless, truncated zoned and sector zoned cores 50%	well-developed planar zoning around cores	3468±2		3524±6	3308±3	3454±4	3476±6
												3472±5	3449±4
T94/221	747.9E, 7582.5S	fine-grained biotite granodiorite gneiss complexely deformed and recrystallized	expected to be older than SRSZ	short prismatic	3.6-2.4	truncated zoned, featureless and sector zoned cores 50%	planar zoning around cores	3451±1	3427±5		3359±11	3466±5	3433±7
												3452±6	3454±7
												3177±2	3416±7
T94/222	747.9E, 7582.5S	coarse-grained quartz diorite, weakly foliated and recrystallized	relation to gray gneiss ?	oval to short prismatic	2.5-1.7	no cores	homogeneous sector zoned	3463±2	3419±8				
T94/227	767.6E, 7621.2S	mylonite in granite/ granodiorite	maximum age of SRSZ	variable, often small long prismatic	variable	zoned truncated cores 10%	sector zoned and planar zoned	3469±3	3440±5	3509±15		3469±8	3475±4
									3415±4			3449±8	3077±6

[a]Australian 1000 m. universal time meridian map grid

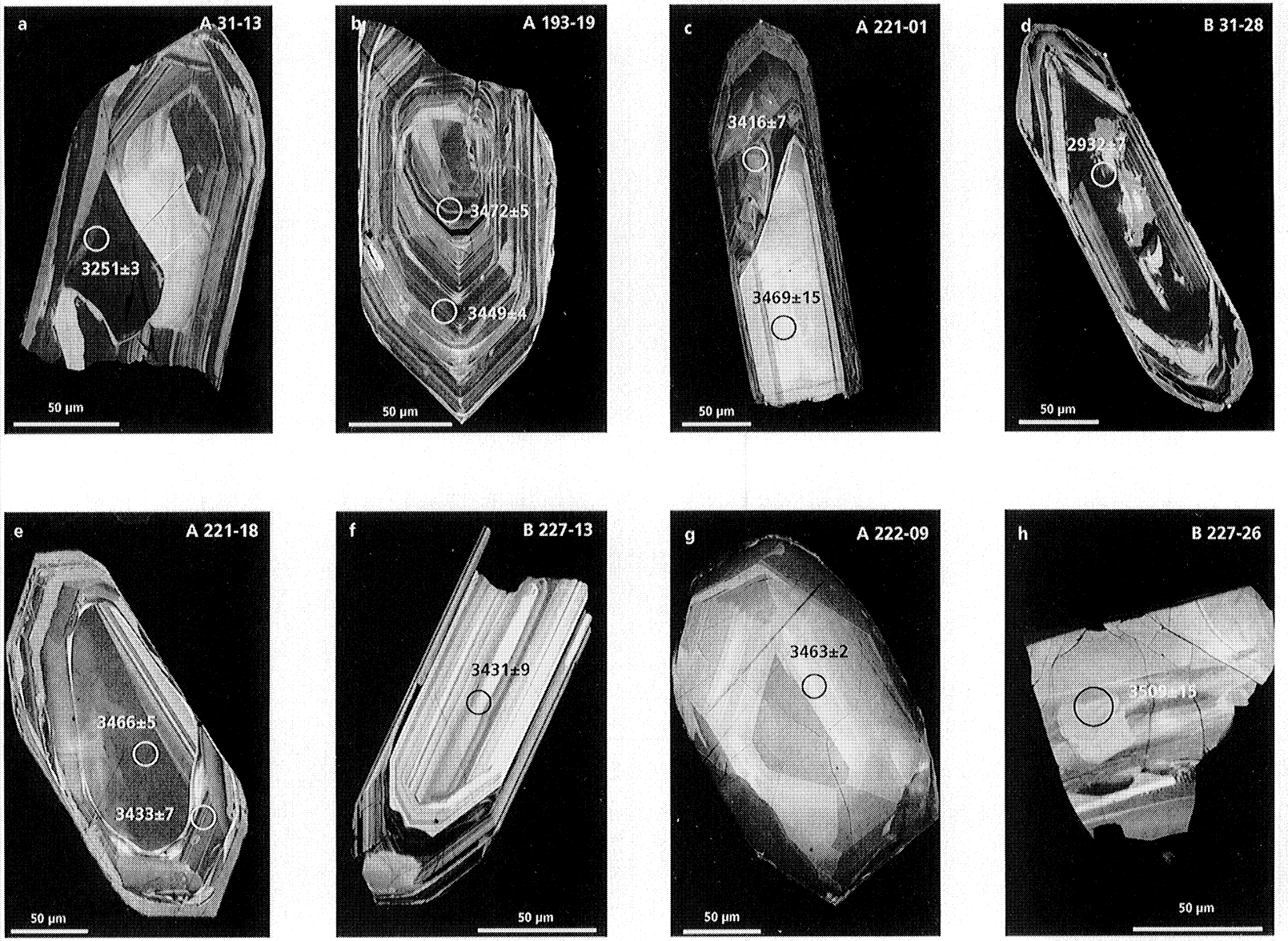

Figure 5. Cathodoluminescence photographs of zircons. Scale bars and the single spot U-Pb ages are indicated. (a) Texture of a partly recrystallized zircon. (b, c, and e) Zircons with older cores and younger rims. (g) A typical zircon from the diorite with sector zoning. (h) One of the two older than 3.45 Ga xenocrystic zircons. The first three numbers in the right-hand corners correspond to the sample number.

Table 2a. Ion Microprobe Analytical Results for Sample T94/31, Synkinematic Granitic Dyke in the Mulgandinnah Shear Zone Complex[a]

Labels	Grain Type	U, ppm	Th, ppm	Pb, ppm	f206,[b] %	$^{207}Pb/^{206}Pb$[c]	1σ	$^{208}Pb/^{206}Pb$	1σ	$^{206}Pb/^{238}U$	1σ	$^{207}Pb/^{235}U$	1σ	Conc. %	$^{207}Pb/^{206}Pb$ date, Ma	1σ	Pool
A3114.1	pl. zoned	205	78	134	0.010	0.21513	0.00081	0.10555	0.00079	0.57579	0.01027	17.079	0.31903	100	2945	6	2934±2
A3103.1	featureless core	691	200	441	0.035	0.21464	0.00048	0.07831	0.00044	0.57288	0.01005	16.954	0.30446	99	2941	4	2934±2
A3119.1	pl.zoned	241	103	155	0.036	0.21449	0.00077	0.11714	0.00091	0.56006	0.00992	16.563	0.30646	98	2940	6	2934±2
A3102.2	pl.zoned rim	312	132	177	0.690 [d]	0.21406	0.00093	0.09642	0.00153	0.49077	0.00868	14.485	0.27125	88	2937[e]	7	2934±2
A3117.1	featureless core	375	173	242	0.029	0.21414	0.00064	0.12552	0.00073	0.55918	0.00987	16.510	0.30164	97	2937	5	2934±2
B3122.1	pl. zoned rim	374	146	235	0.222	0.21367	0.00087	0.10605	0.00119	0.55055	0.01786	16.220	0.53840	96	2934	7	2934±2
B3128.1	irr. zoned core	656	426	433	0.094	0.21344	0.00061	0.17246	0.00083	0.55089	0.01781	16.212	0.53184	96	2932	5	2934±2
B3105.1	pl.zoned	338	180	254	0.045	0.21316	0.00076	0.13655	0.00093	0.64566	0.00688	18.976	0.22116	110	2930	6	2934±2
B3133.1	irr. zoned	500	215	314	0.353 [d]	0.21296	0.00079	0.11820	0.00115	0.54204	0.01755	15.916	0.52609	95	2928	6	2934±2
A3101.1	irr. zoned	588	317	392	0.019	0.21296	0.00045	0.14613	0.00051	0.56853	0.00997	16.694	0.29907	99	2928	3	2934±2
A3118.1	featureless core	234	75	103	1.095 [d]	0.21167	0.00131	0.12228	0.00237	0.36965	0.00653	10.788	0.20976	69	2918[f]	10	2934±2
B3125.1	irr. zoned	862	431	580	0.037	0.21118	0.00058	0.13407	0.00074	0.58068	0.01877	16.908	0.55422	101	2915	4	2911±4
A3102.1	featureless core	308	123	210	0.102	0.21046	0.00070	0.10666	0.00086	0.59870	0.01061	17.373	0.32015	104	2909[f]	5	2911±4
B3111.1	sector zoned	358	155	191	0.182	0.20892	0.00156	0.11082	0.00231	0.46601	0.00520	13.424	0.19035	85	2897	12	2911±4
B3123.1	pl. zoned core	327	212	297	0.265	0.29307	0.00102	0.16919	0.00131	0.71729	0.02330	28.985	0.95916	102	3434[f]	5	
B3101.1	dirty core	534	12	419	0.146 [d]	0.28969	0.00067	0.00628	0.00054	0.69970	0.00725	27.948	0.30437	100	3416	4	
B3106.1	irr.zoned	1083	970	939	0.221 [d]	0.28764	0.00051	0.24590	0.00071	0.65164	0.00666	25.843	0.27364	95	3405	3	
B3134.1	pl. zoned	995	260	791	0.029	0.28745	0.00050	0.06808	0.00034	0.68099	0.02199	26.990	0.87862	98	3404	3	
A3115.1	featureless core	1053	169	876	0.058	0.28624	0.00039	0.04360	0.00026	0.72555	0.01269	28.635	0.50710	104	3397	2	
B3123.2	irr. zoned rim	955	214	701	0.076	0.28110	0.00053	0.05394	0.00039	0.63779	0.02059	24.720	0.80531	94	3369[e]	3	
A3113.1	recryst. core	793	23	551	0.070	0.26063	0.00047	0.00811	0.00035	0.63476	0.01112	22.811	0.40660	97	3251[g]	3	
B3107.1	irr.zoned	507	110	341	1.234 [d]	0.25968	0.00099	0.09292	0.00169	0.55275	0.00575	19.791	0.22788	87	3245	6	
B3132.1	irr. zoned	871	4	562	0.062	0.23434	0.00054	0.00038	0.00038	0.60619	0.01958	19.586	0.63974	99	3082	4	
B3104.1	pl.zoned rim	369	60	250	0.396 [d]	0.23317	0.00086	0.05724	0.00116	0.60092	0.00632	19.319	0.22347	99	3074	6	
A3109.1	irr.zoned	110	22	69	0.057	0.21999	0.00133	0.05777	0.00172	0.57097	0.01035	17.319	0.34311	98	2981	10	
A3118.2	pl.zoned rim	2857	119	420	0.398 [d]	0.10450	0.00036	0.01240	0.00061	0.15091	0.00263	2.174	0.03952	53	1705[e,h]	6	

[a]Defintitions are as follows: Conc., concordance, equal to 100x ($^{206}Pb/^{238}U$ age)/($^{207}Pb/^{206}Pb$ age); pool, pooled age group; pl., planar; irr., irregular; recryst., recrystallized

[b]Equal to 100 (common ^{206}Pb/total ^{206}Pb)

[c]Ratios corrected for common Pb using the measured ^{204}Pb abundance

[d]Analyses for which common Pb correction was made, using *Cumming and Richard* [1975]

[e]Rim

[f]Core

[g]Recrystallized

[h]Unreliable

Table 2b. Ion Microprobe Analytical Results for Sample T94/193, North Shaw Granodiorite From the Eastern Shaw Granitoid Complex[a]

Labels	Grain Type	U, ppm	Th, ppm	Pb, ppm	f206,[b] %	$^{207}Pb/^{206}Pb$[c]	1σ	$^{208}Pb/^{206}Pb$	1σ	$^{206}Pb/^{238}U$	1σ	$^{207}Pb/^{235}U$	1σ	Conc. %	$^{207}Pb/^{206}Pb$ date, Ma	1σ	Pool
B19322.1	pl. zoned core	333	370	311	0.142	0.31059	0.00114	0.32348	0.00160	0.65905	0.03551	28.223	1.53693	93	3524	6	
A19303.2	pl. zoned rim	165	162	156	0.093	0.30117	0.00108	0.26224	0.00143	0.70062	0.01263	29.094	0.54749	98	3476[e]	6	3468±2
A19315.1	featureless core	286	269	232	0.450	0.30049	0.00097	0.23224	0.00141	0.60694	0.01077	25.146	0.46336	88	3473	5	3468±2
A19319.1	irr. zoned core	276	273	261	0.066	0.30035	0.00104	0.26660	0.00141	0.69854	0.01252	28.929	0.54041	98	3472f	5	3468±2
A19321.2	pl. zoned core	95	40	84	0.079	0.30001	0.00146	0.11228	0.00141	0.72433	0.01336	29.962	0.58889	101	3470f	8	3468±2
A19321.1	pl. zoned core	72	60	68	0.048	0.29956	0.00185	0.21868	0.00258	0.71223	0.01358	29.418	0.61056	100	3468e	10	3468±2
A19322.1	pl. zoned core	110	150	110	0.052	0.29920	0.00133	0.36347	0.00205	0.69887	0.01279	28.831	0.55821	99	3466	7	3468±2
A19309.1	pl. zoned	314	229	295	0.031	0.29861	0.00075	0.19393	0.00082	0.73213	0.01298	30.143	0.54906	102	3463	4	3468±2
A19318.1	sector zoned core	114	125	110	0.069	0.29827	0.00135	0.28887	0.00192	0.70667	0.01296	29.062	0.56486	100	3461	7	3468±2
A19310.1	sector zoned	134	206	138	0.035	0.29803	0.00124	0.40816	0.00206	0.69986	0.01269	28.759	0.54935	99	3460	6	3468±2
B19327.1	pl. zoned core	235	352	238	0.074	0.29727	0.00114	0.39496	0.00188	0.69374	0.02259	28.434	0.94592	98	3456[f]	6	
A19303.1	dirty core	320	493	326	0.068	0.29692	0.00074	0.40136	0.00120	0.69400	0.01228	28.411	0.51627	98	3454[f]	4	
A19319.2	pl. zoned rim	312	338	303	0.051	0.29591	0.00078	0.28587	0.00103	0.71025	0.01259	28.978	0.52874	100	3449[e]	4	
A19301.1	pl. zoned core	278	237	183	0.552 [d]	0.29394	0.00110	0.29927	0.00185	0.47117	0.00834	19.095	0.35424	72	3439	6	
B19321.1	irr. zoned	393	136	276	0.126	0.28991	0.00084	0.09692	0.00085	0.58516	0.03149	23.391	1.26903	87	3417	5	
A19323.1	dirty core	314	219	242	0.672	0.28846	0.00121	0.21917	0.00194	0.58245	0.01039	23.165	0.43597	87	3409	7	
A19324.1	pl. zoned rim	502	240	400	0.053	0.27036	0.00058	0.12581	0.00056	0.66147	0.01164	24.658	0.44376	99	3308	3	
B19327.2	pl. zoned rim	439	103	253	0.194	0.26861	0.00090	0.07552	0.00096	0.49589	0.01608	18.366	0.60629	79	3298[e]	5	
B19340.1	pl. zoned rim	367	159	269	0.068	0.26521	0.00087	0.11298	0.00091	0.61611	0.03317	22.529	1.22455	94	3278	5	
A19329.1	pl. zoned rim	496	333	374	0.095	0.26048	0.00063	0.17709	0.00079	0.60845	0.01071	21.852	0.39450	94	3250	4	
B19328.1	irr. zoned	522	78	291	0.335 [d]	0.25770	0.00089	0.04661	0.00105	0.49027	0.01587	17.420	0.57446	80	3233	5	
A19308.1	featureless core	539	211	383	0.122	0.25509	0.00061	0.10840	0.00066	0.60314	0.01062	21.214	0.38305	95	3217[g]	4	
A19312.1	pl. zoned	721	395	486	0.073	0.25098	0.00051	0.15149	0.00058	0.55683	0.00976	19.269	0.34504	89	3191	3	
B19308.1	pl. zoned	716	825	416	0.503 [d]	0.24458	0.00083	0.28792	0.00145	0.43287	0.01399	14.598	0.48048	74	3150[f,g]	5	
A19308.2	pl. zoned rim	600	348	267	0.206	0.22383	0.00067	0.15182	0.00096	0.37371	0.00656	11.533	0.20947	68	3008[e,h]	5	
B19336.1	pl. zoned	728	352	331	0.263	0.21932	0.00069	0.13439	0.00099	0.38733	0.02083	11.713	0.63538	71	2976[h]	5	
B19337.1	featureless core	1118	621	609	0.388 [d]	0.20774	0.00056	0.15925	0.00089	0.45656	0.02454	13.077	0.70807	84	2888[h]	4	
A19326.1	pl. zoned rim	979	700	431	0.357 [d]	0.18953	0.00054	0.20605	0.00092	0.36186	0.00633	9.456	0.17092	73	2738[h]	5	
A19313.1	pl. zoned	1145	939	424	0.211	0.16316	0.00045	0.21401	0.00080	0.31057	0.00543	6.987	0.12607	70	2489[h]	5	

[a]Defintitions are as follows: Conc., concordance, equal to 100x ($^{206}Pb/^{238}U$ age)/($^{207}Pb/^{206}Pb$ age); pool, pooled age group; pl., planar; irr., irregular; recryst., recrystallized

[b]Equal to 100 (common ^{206}Pb/total ^{206}Pb)

[c]Ratios corrected for common Pb using the measured ^{204}Pb abundance

[d]Analyses for which common Pb correction was made, using *Cumming and Richard* [1975]

[e]Rim

[f]Core

[g]Recrystallized

[h]Unreliable

Table 2c. Ion Microprobe Analytical Results for Sample T94/221, Gray Migmatic Gneiss From the Central Shaw Granitoid Complex[a]

Labels	Grain Type	U, ppm	Th, ppm	Pb, ppm	f206,[b] %	$^{207}Pb/^{206}Pb$[c]	1σ	$^{208}Pb/^{206}Pb$	1σ	$^{206}Pb/^{238}U$	1σ	$^{207}Pb/^{235}U$	1σ	Conc. %	$^{207}Pb/^{206}Pb$ date, Ma	1σ	Pool
A22101.1	featureless core	54	23	46	0.107	0.29980	0.00285	0.11314	0.00431	0.68934	0.00950	28.495	0.50420	97	3469	15	3451±1
B22123.1	sector zoned core	35	16	30	0.064	0.29811	0.00217	0.12081	0.00255	0.71669	0.01794	29.458	0.79355	101	3460	11	3451±1
B22121.1	pl. zoned core	39	15	24	0.848	0.29744	0.00302	0.07805	0.00500	0.51275	0.01263	21.029	0.58460	77	3457	16	3451±1
B22125.1	irr. zoned	222	135	196	0.053	0.29698	0.00080	0.16225	0.00085	0.70210	0.01667	28.749	0.69642	99	3455	4	3451±1
A22112.2	irr. zoned rim	207	29	136	0.012	0.29694	0.00139	0.03617	0.00149	0.57261	0.00644	23.443	0.29816	84	3454[e]	7	3451±1
B22142.1	pl. zoned	269	332	266	0.044	0.29691	0.00070	0.32633	0.00103	0.70503	0.01670	28.862	0.69533	100	3454	4	3451±1
A22112.1	featureless core	209	68	174	0.042	0.29647	0.00115	0.08442	0.00103	0.69788	0.00769	28.528	0.34578	99	3452[f]	6	3451±1
B22132.1	featureless core	291	151	257	0.044	0.29612	0.00068	0.13292	0.00065	0.71875	0.01703	29.346	0.70698	101	3450	4	3451±1
B22104.1	zoned core	726	356	638	0.063	0.29620	0.00042	0.12839	0.00040	0.71579	0.01688	29.233	0.69555	101	3450	2	3451±1
B22146.1	irr. zoned	282	76	236	0.033	0.29569	0.00066	0.07415	0.00055	0.70928	0.01679	28.917	0.69548	100	3448	3	3451±1
B22150.1	pl. zoned core	54	29	50	0.186	0.29560	0.00196	0.14757	0.00272	0.74180	0.01834	30.234	0.79757	104	3447	10	3451±1
B22149.1	pl. zoned core	214	233	209	-0.004	0.29513	0.00081	0.31364	0.00115	0.70272	0.01669	28.595	0.69344	100	3445	4	3451±1
B22134.1	pl. zoned core	141	76	121	0.122	0.29358	0.00140	0.13991	0.00181	0.69064	0.01660	27.956	0.70132	98	3437	7	3427±5
A22118.2	irr. zoned rim	312	141	247	0.290	0.29282	0.00130	0.11804	0.00168	0.64583	0.00699	26.075	0.31813	94	3433[e]	7	3427±5
B22110.1	pl. zoned core	219	115	210	-0.104	0.29063	0.00185	0.13252	0.00270	0.78666	0.01906	31.523	0.81344	109	3421	10	3427±5
A22101.2	featureless rim	196	42	173	0.159	0.28967	0.00136	0.05367	0.00134	0.75694	0.00850	30.232	0.38374	106	3416[e]	7	3427±5
A22118.1	pl. zoned core	374	671	438	0.025	0.29924	0.00091	0.47318	0.00157	0.76617	0.00818	31.612	0.36201	106	3466[f]	5	
B22148.1	irr. zoned	263	107	198	0.216	0.28674	0.00129	0.10152	0.00155	0.62662	0.01495	24.774	0.61507	92	3400	7	
B22109.1	featureless cor	207	96	196	0.108[d]	0.27934	0.00188	0.10512	0.00255	0.78972	0.01913	30.417	0.78886	112	3359[g]	11	
B22101.1	featureless cor	1228	580	792	0.082	0.24873	0.00034	0.12461	0.00037	0.54405	0.01281	18.658	0.44327	88	3177[h]	2	
B22103.1	zoned core	1991	6605	1063	0.418[d]	0.18339	0.00036	0.88562	0.00117	0.29615	0.00697	7.488	0.17860	62	2684[h]	3	

[a]Defintitions are as follows: Conc., concordance, equal to 100x ($^{206}Pb/^{238}U$ age)/($^{207}Pb/^{206}Pb$ age); pool, pooled age group; pl., planar; irr., irregular; recryst., recrystallized

[b]Equal to 100 (common ^{206}Pb/total ^{206}Pb)

[c]Ratios corrected for common Pb using the measured ^{204}Pb abundance

[d]Analyses for which common Pb correction was made, using *Cumming and Richard* [1975]

[e]Rim

[f]Core

[g]Recrystallized

[h]Unreliable

Table 2d. Ion Microprobe Analytical Results for Sample T94/222, Dioritic Gneiss From the Central Shaw Granitoid Complex[a]

Labels	Grain Type	U, ppm	Th, ppm	Pb, ppm	f206,[b] %	$^{207}Pb/^{206}Pb$[c]	1σ	$^{208}Pb/^{206}Pb$	1σ	$^{206}Pb/^{238}U$	1σ	$^{207}Pb/^{235}U$	1σ	Conc. %	$^{207}Pb/^{206}Pb$ date, Ma	1σ	Pool
B22b34.1	sector zoned	135	132	126	0.025	0.30008	0.00102	0.26178	0.00128	0.69541	0.01660	28.772	0.70558	98	3471	5	3463±2
B22b30.1	sector zoned	92	99	93	0.063	0.29992	0.00146	0.28483	0.00199	0.74035	0.01802	30.615	0.77763	103	3470	8	3463±2
B22b25.1	sector zoned	113	125	109	0.003	0.29963	0.00135	0.29789	0.00173	0.69810	0.01698	28.841	0.72909	98	3468	7	3463±2
B22b33.1	sector zoned	176	197	171	0.011	0.29957	0.00090	0.29774	0.00117	0.70800	0.01686	29.244	0.71263	100	3468	5	3463±2
A22210.1	sector zoned	121	116	122	-0.015	0.29924	0.00163	0.25395	0.00227	0.74941	0.00903	30.920	0.42762	104	3466	8	3463±2
B22b15.1	sector zoned	134	175	160	0.192	0.29877	0.00165	0.33636	0.00265	0.84215	0.01434	34.691	0.64323	114	3464	9	3463±2
B22b28.1	sector zoned	137	142	130	0.169	0.29887	0.00124	0.27481	0.00170	0.69749	0.01672	28.742	0.71383	98	3464	6	3463±2
B22b37.1	sector zoned	135	117	121	0.000	0.29851	0.00132	0.22525	0.00142	0.68113	0.01641	28.035	0.70169	97	3463	7	3463±2
B22b21.1	sector zoned	134	151	114	-0.020	0.29839	0.00278	0.30921	0.00390	0.61609	0.01579	25.348	0.71834	89	3462	14	3463±2
B22b35.1	sector zoned	96	95	91	0.020	0.29804	0.00120	0.26301	0.00158	0.70299	0.01688	28.889	0.71756	99	3460	6	3463±2
A22207.1	sector zoned	90	97	86	0.276	0.29782	0.00215	0.28928	0.00344	0.69733	0.00876	28.634	0.43648	99	3459	11	3463±2
B22b36.1	sector zoned	115	112	107	0.105	0.29782	0.00116	0.25612	0.00160	0.69764	0.01672	28.648	0.70938	99	3459	6	3463±2
B22b27.1	sector zoned	118	110	107	0.100	0.29685	0.00114	0.24684	0.00150	0.68135	0.01628	27.887	0.68791	97	3454	6	3463±2
B22b14.1	sector zoned	115	115	121	0.044	0.29613	0.00105	0.24818	0.00134	0.79023	0.01291	32.265	0.55310	109	3450	5	3463±2
B22b18.1	sector zoned	104	62	102	-0.022	0.29174	0.00257	0.15466	0.00278	0.78742	0.01990	31.674	0.87999	109	3427	14	3419±8
B22b20.1	sector zoned	256	333	225	0.212	0.29144	0.00161	0.32635	0.00255	0.62548	0.01499	25.134	0.63504	91	3425	9	3419±8
B22b22.1	sector zoned	94	74	95	0.005	0.28718	0.00223	0.19654	0.00230	0.78336	0.01961	31.018	0.84119	110	3402	12	3419±8

[a]Defintitions are as follows: Conc., concordance, equal to 100x ($^{206}Pb/^{238}U$ age)/($^{207}Pb/^{206}Pb$ age); pool, pooled age group; pl., planar; irr., irregular; recryst., recrystallized

[b]Equal to 100 (common ^{206}Pb/total ^{206}Pb)

[c]Ratios corrected for common Pb using the measured ^{204}Pb abundance

Table 2e. Ion Microprobe Analytical Results for Sample T94/227, Split Rock Shear Zone Mylonite From Eastern Shaw Granitoid Complex[a]

Labels	Grain Type	U, ppm	Th, ppm	Pb, ppm	f206,[b] %	$^{207}Pb/^{206}Pb$[c]	1σ	$^{208}Pb/^{206}Pb$	1σ	$^{206}Pb/^{238}U$	1σ	$^{207}Pb/^{235}U$	1σ	Conc. %	$^{207}Pb/^{206}Pb$ date, Ma	1σ	Pool
B22726.1	partly recryst.	38	18	36	0.338	0.30756	0.00304	0.11604	0.00441	0.76316	0.02351	32.363	1.08414	104	3509	15	
B22706.2	sector zoned rim	435	105	330	0.281 [d]	0.30096	0.00085	0.06625	0.00094	0.63892	0.04158	26.513	1.73633	92	3475[e]	4	3469±3
B22706.1	sector zoned core	113	85	100	0.091	0.29976	0.00154	0.19996	0.00188	0.68771	0.04492	28.424	1.88018	97	3469[f]	8	3469±3
B22724.1	sector zoned	141	186	153	0.001	0.29907	0.00142	0.35027	0.00200	0.76664	0.05008	31.613	2.08924	106	3465	7	3469±3
A22703.1	sector zoned	105	109	106	0.126	0.29871	0.00143	0.27368	0.00201	0.74031	0.01366	30.490	0.59850	103	3464	7	3469±3
B22711.1	sector zoned	234	217	214	0.154	0.29820	0.00126	0.23882	0.00170	0.68580	0.02004	28.197	0.84706	97	3461	7	3469±3
A22707.1	sector zoned	127	103	121	0.174	0.29594	0.00145	0.22930	0.00195	0.72405	0.01336	29.544	0.58127	102	3449[f]	8	3440±5
B22719.1	sector zoned	101	95	99	0.047	0.29470	0.00176	0.24354	0.00247	0.73871	0.02197	30.017	0.93215	104	3443	9	3440±5
A22706.1	sector zoned	93	89	84	0.482	0.29291	0.00297	0.24167	0.00506	0.67566	0.01325	27.288	0.63236	97	3433	16	3440±5
B22731.1	sector zoned	115	92	95	0.178	0.29252	0.00166	0.22478	0.00231	0.62789	0.01850	25.324	0.77745	92	3431	9	3440±5
A22705.1	sector zoned	119	116	111	0.068	0.29209	0.00292	0.24553	0.00455	0.70710	0.01361	28.477	0.64841	101	3429	16	3440±5
B22718.1	pl. zoned	868	560	693	0.269 [d]	0.29023	0.00058	0.19557	0.00077	0.61834	0.04022	24.743	1.61621	91	3419	3	3415±4
B22707.1	pl. zoned core	222	178	164	0.369	0.28821	0.00125	0.16398	0.00174	0.58380	0.01702	23.199	0.69617	87	3408	7	3415±4
A22702.1	pl. zoned	133	72	100	0.625	0.28760	0.00156	0.18055	0.00238	0.58288	0.01059	23.114	0.45311	87	3405	8	3415±4
A22704.1	sector zoned	138	147	122	0.321 [d]	0.28699	0.00339	0.25055	0.00581	0.66068	0.01276	26.143	0.62381	96	3401	18	3415±4
A22701.1	recryst. core	181	145	212	1.550 [d]	0.27543	0.00148	0.29667	0.00281	0.82722	0.01500	31.414	0.61381	116	3337[h]	8	
B22714.1	pl. zoned	117	50	155	2.683 [d]	0.26001	0.00205	0.20853	0.00405	0.95785	0.02830	34.339	1.08225	133	3247[h]	12	
B22707.2	featureless rim	706	7332	1744	5.367 [d]	0.23359	0.00089	0.32157	0.00193	1.56427	0.04560	50.381	1.50474	197	3077[e,h]	6	
B22708.1	dirty core	329	5	124	0.043	0.12529	0.00076	0.00457	0.00081	0.38677	0.01122	6.681	0.20284	104	2033[h]	11	

[a]Defintitions are as follows: Conc., concordance, equal to 100x ($^{206}Pb/^{238}U$ age)/($^{207}Pb/^{206}Pb$ age); pool, pooled age group; pl., planar; irr., irregular; recryst., recrystallized

[b]Equal to 100 (common ^{206}Pb/total ^{206}Pb)

[c]Ratios corrected for common Pb using the measured ^{204}Pb abundance

[d]Analyses for which common Pb correction was made, using *Cumming and Richard* [1975]

[e]Rim

[f]Core

[g]Recrystallized

[h]Unreliable

cores (Figures 5a and 5d). An unusual texture found in some zircon domains is shown in Figure 5a. The growth zonation has almost disappeared in the core and this region is subdivided into three featureless domains. The boundary between the core region and the zoned rim is gradational in some areas but sharp in others. This texture is reminiscent of the recrystallization texture previously described by *Pidgeon* [1992]. Growth zoning can be sharp and planar as shown in the rim of Figure 5b, or locally irregular as illustrated in Figure 5d.

Twenty-six analyses were obtained from the zircons from sample T94/31, with three zircons analyzed at two sites. Most analyses plot close to the concordia curve, with the discordance pattern mostly consistent with recent loss of radiogenic Pb from the analysis sites (Figure 6a). Fifteen analyses have $^{207}Pb/^{206}Pb$ ages ranging from 2945 to 2909 Ma. Eleven concordant and normally discordant analyses have $^{207}Pb/^{206}Pb$ ratios within error of a single weighted mean value corresponding to a $^{207}Pb/^{206}Pb$ date of 2934±2 Ma (chi^2= 1.37). This date is interpreted as corresponding to the time of igneous crystallization of the granitic dyke. Three analyses give a slightly younger weighted mean date of 2911±4 Ma, but all are reverse discordant, indicating U loss, or gain of radiogenic Pb, at these analysis sites. The remaining analyses give older $^{207}Pb/^{206}Pb$ dates ranging from 3434 to 2981 Ma and are interpreted to be of xenocryst zircons.

Of the three zircons that were analyzed at two sites (Tables 1 and 2), one grain (A3102) had a younger core date (2909±5 Ma) than the rim (2937±7 Ma), possibly indicating recrystallization of the core. Two analyses of the zircon B3123, interpreted as a xenocryst, indicated that the core crystallized at 3434±5 Ma and the rim at 3369±3 Ma. Zircon A3118 has a core that crystallized within the pooled 2934±2 Ma group, but the analysis of the rim indicated an anomalously young date, probably due to radiogenic Pb loss caused by radioactive damage due to the very high U content (2857 ppm). Zircon A3113, with an internal texture suggesting recrystallization of the core (Figure 5a), gave a concordant $^{207}Pb/^{206}Pb$ date of 3251±3 Ma.

4.2. T94/193 Syn-Split Rock Shear Zone Granodiorite

This sample contained short prismatic, planar zoned, light brown zircons with rounded cores. Planar growth zones are well developed in these zircons (Figure 5b). Some cores are sector zoned and resemble zircons from sample T94/222 (Figure 5g). Twenty-six analyses were obtained on zircons from sample T94/193, with five zircon grains analyzed at two sites. The discordance pattern is consistent with several episodes of radiogenic Pb loss, including a recent radiogenic Pb loss event, from the analysis sites. Thirteen concordant analyses have $^{207}Pb/^{206}Pb$ ratios within error of a single value, corresponding to a weighted mean $^{207}Pb/^{206}Pb$ date of circa 3460 Ma. One concordant analysis (B19322.1) indicated a distinctly older $^{207}Pb/^{206}Pb$ date (3524±6 Ma), whereas the remaining highly discordant analyses indicated younger $^{207}Pb/^{206}Pb$ dates and are interpreted to be of sites from which some accumulated radiogenic Pb has been lost since crystallization.

Pooling the 13 concordant analyses gives a weighted mean $^{207}Pb/^{206}Pb$ date of 3462± 3 Ma, with the scatter of analyses about the mean value in excess of that expected from analytical sources of error alone (chi^2=2.66). Deletion of the three youngest points results in a weighted mean $^{207}Pb/^{206}Pb$ date of 3468±2 Ma (chi^2= 0.87). This is interpreted as the time of crystallization of the granodiorite. The older analysis (B19322.1) with a $^{207}Pb/^{206}Pb$ date of 3524±6 Ma, is interpreted to be of a xenocrystic zircon.

Of the remaining analyses, the six youngest, with $^{207}Pb/^{206}Pb$ dates between 3150 and 2489 Ma, have high U contents (>1000 ppm) and are highly discordant. For analyses with U contents less than 350 ppm, $^{207}Pb/^{206}Pb$ dates are circa 3250 Ma, but $^{207}Pb/^{206}Pb$ dates obtained for analyses having U>500 ppm are negatively correlated with U contents at the analysis sites. These sites are interpreted to have lost some of their accumulated radiogenic Pb since crystallization. Similar trends in $^{207}Pb/^{206}Pb$ data versus U concentration for the other samples suggest that a threshold value of ~500 ppm U, above which $^{207}Pb/^{206}Pb$ dates are not reliable because of redistribution of radiogenic Pb within individual zircon crystals, might apply for this region of the Pilbara Craton. A similar threshold value was reported by *Nelson* [1997b] for SHRIMP U-Pb zircon analyses obtained on samples from the Yilgarn Craton. The circa 3250 Ma group does not show this behavior and their $^{207}Pb/^{206}Pb$ dates are interpreted as providing the time of new growth and recrystallization of zircon during a metamorphic event at circa 3250 Ma. One analysis (A19324.1) in this group is concordant and indicates a $^{207}Pb/^{206}Pb$ date of 3308 Ma.

Of the multiple analyses obtained on individual zircons, those of zircon A19303 indicate a slightly younger $^{207}Pb/^{206}Pb$ date for the core (3454±4 Ma) than the rim (3476±6 Ma). For zircon A19319 (Figure 5) the $^{207}Pb/^{206}Pb$ date on the core was 3472±5 Ma, whereas that of the rim was 3449±6 Ma. Analyses of both these grains plot within the concordant group, with a slightly younger date than the 3468±2 Ma age group. Two analyses of zircon A19321 agree within error.

4.3. T94/221 Gray Gneiss of the Central Shaw Complex

This sample contained short prismatic, planar zoned, light brown zircons with rounded cores. The cores are either planar zoned, featureless, or sector zoned (Figures 5d-5g). Twenty-one analyses were obtained from the zircons of granodiorite sample T94/221, with three zircons analyzed at two sites. The discordance pattern is consistent with several episodes of radiogenic Pb redistribution, including a recent radiogenic Pb redistribution event, from the analysis sites. The analyses show one distinct concordant group with a weighted mean $^{207}Pb/^{206}Pb$ date of 3451±1 Ma (chi^2= 0.62). This is interpreted as corresponding to the time of crystallization of the granodiorite. The remaining analyses are either discordant or reversely discordant and indicate $^{207}Pb/^{206}Pb$ dates as young as 3359 Ma. Four of these analyses have $^{207}Pb/^{206}Pb$ ratios within error of a single value, corresponding to a weighted mean $^{207}Pb/^{206}Pb$ date of 3427±5 Ma (chi^2= 1.35). Two analyses, with U contents higher than 1000 ppm, are highly discordant and are interpreted to be of sites from which some radiogenic Pb has been lost since crystallization.

The two analyses obtained on zircon A22112 are analytically indistinguishable. A date of 3466±5 Ma was obtained for the core of zircon A22118 (Figure 5e), whereas the rim analysis of this grain indicated a date of 3433±7 Ma. For zircon A22101 a date of 3416±7 Ma was obtained on the rim. The core analysis indicated a date of 3177±2 Ma, but its high U content of 1228 ppm and high degree of discordance indicates that this analysis site has lost some of its accumulated radiogenic Pb since crystallization.

4.4. T94/222 Diorite of the Central Shaw Complex

The zircons from this sample are oval to short prismatic and all show the characteristic sector zoning texture (Figure 5g). They show no cores or other textural inhomogeneities. Seventeen analyses were obtained from 17 zircons. Fourteen of these analyses have $^{207}Pb/^{206}Pb$ ratios within error of a single value.

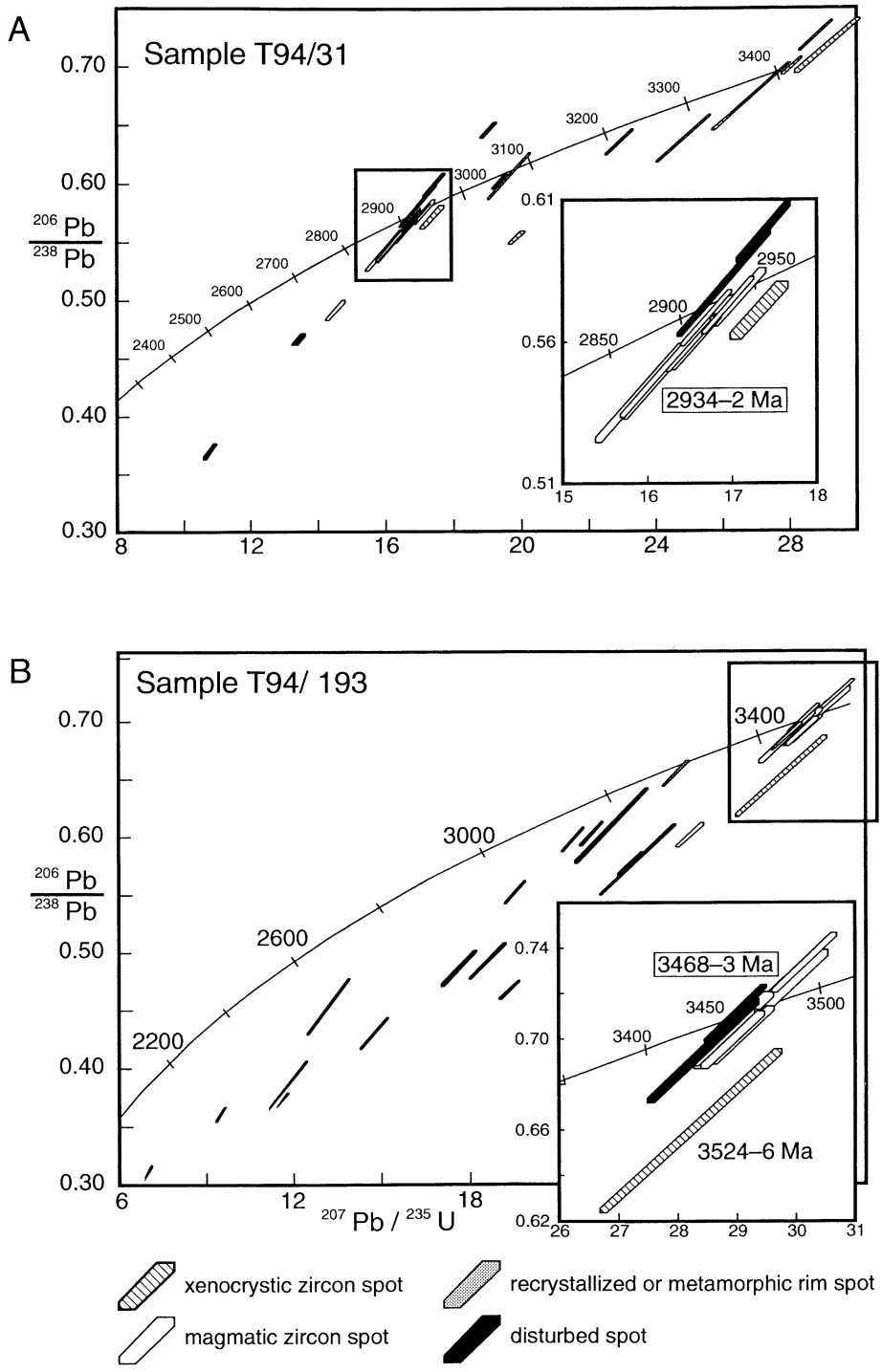

Figure 6. Concordia diagrams of samples dated in this study. All error boxes are 2 σ, framed ages are crystallization ages, and unframed ages represent other pooled ages; see text for discussion.

These analyses plot close to the concordia, but some are slightly normally or reversely discordant. The weighted mean $^{207}Pb/^{206}Pb$ date for this group, 3463±2 Ma (chi^2= 0.96), is interpreted as the time of igneous crystallization of the diorite.

Three discordant analyses indicate a slightly younger weighted mean $^{207}Pb/^{206}Pb$ date of 3419±8 Ma. There are no obvious morphological or chemical differences between the zircons belonging to the two groups, suggesting that the younger date may correspond to the time of a metamorphic disturbance event during which zircons, which crystallized at 3463 Ma, lost some of their accumulated radiogenic Pb. The sample was homogeneous and there were no other igneous phases, such as veins or inclusions, that may explain the occurrence of the younger age group.

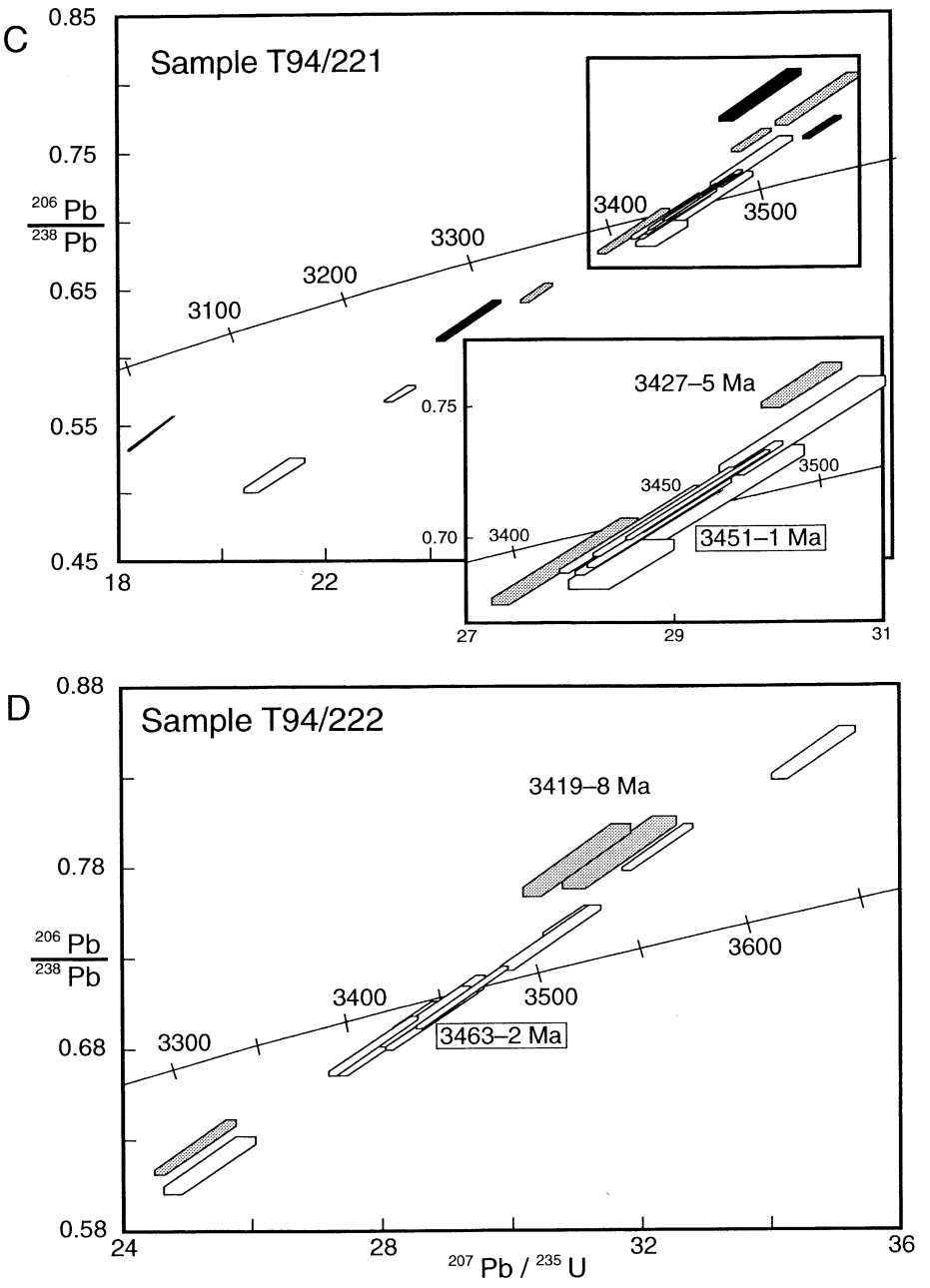

Figure 6. (continued)

4.5. T94/227 Mylonite From the SRSZ

The zircons from this sample were commonly < 30 μm in diameter. The smaller, brown zircons have a long prismatic shape. The larger zircons vary in shape from elongate and prismatic with well-developed crystal faces (Figure 5f) to highly rounded. Some rounded zircons have pitted surfaces. Colors vary from light brown to pink shades. This sample included planar, sector, and irregularly zoned grains, but cores are uncommon. Nineteen analyses were obtained from 17 zircons. Fourteen analyses plot near to the concordia curve and have $^{207}Pb/^{206}Pb$ dates between 3.5 and 3.4 Ga. One analysis (B22716.1) indicated a $^{207}Pb/^{206}Pb$ date >3.5 Ga, whereas the remaining analyses are highly discordant. The >3.5 Ga zircon has an irregular planar texture with a ~25 μm recrystallized and cloudy area truncating the irregular planar texture. The analysis site is partly within the recrystallized zone (Figure 3h). The $^{207}Pb/^{206}Pb$ date of 3509±15 Ma obtained for this site may correspond to a mixed date from both original (xenocryst) and recrystallized zones.

The analyses may be subdivided into three groups with weighted mean $^{207}Pb/^{206}Pb$ dates of 3469±3 Ma (n=5, chi^2= 0.85), 3440±5 Ma (n=5, chi^2= 0.65), and 3415±4 Ma (n=4, chi^2=1.28). The two older groups are mainly from sites located in sector zoned parts of zircons, whereas the youngest group (3415±4 Ma) were obtained on planar-zoned sites. Although there is no chemical difference between the groups, these observations

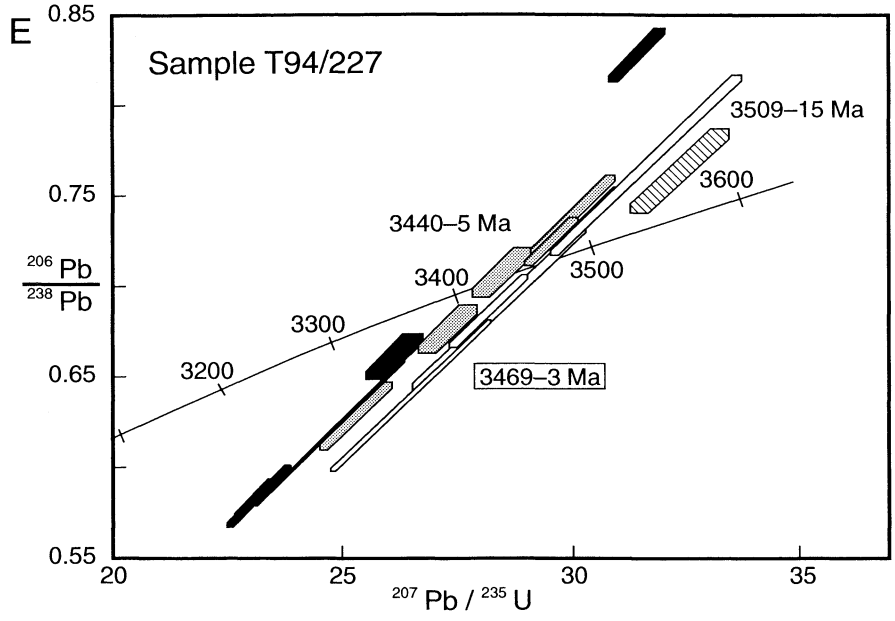

Figure 6. (continued)

suggest that there were several zircon growth and/or recrystallization events. The mylonitic sample contained lithologically distinct layers, which may originally have represented different intrusive phases. The two youngest analyses (B22707.2 and B22708.1) are interpreted to be sites that have lost radiogenic Pb since crystallization.

5. Discussion

5.1. Interpretation of SHRIMP U-Pb Zircon Results

The SHRIMP data are summarized in a series of histogram plots of $^{207}Pb/^{206}Pb$ dates for individual analysis sites in Figure 7. Highly discordant analyses (with >15% discordance) and analyses with high U or Th (U>500 ppm) have not been included since they are regarded as unreliable for reasons outlined in the previous section. The age peaks for samples T94/193, T94/221 and T94/222 are skewed toward lower ages, probably as a result of nonzero age Pb loss.

The oldest major age component is between 3470 and 3400 Ma (Figure 7f). In this range, three age groups can be distinguished. This is reflected in the weighted mean $^{207}Pb/^{206}Pb$ dates obtained for T94/193, T94/222, and T94/227, which belong to the 3465 Ma group, and the weighted mean $^{207}Pb/^{206}Pb$ date obtained for T94/221, which belongs to a second group at circa 3450 Ma (see Table 1 for a summary of data for each sample). Several zircons with distinct cores and rims gave multiple $^{207}Pb/^{206}Pb$ dates of circa 3470 Ma and 3450 Ma. This suggests that the 3450 Ma event represents a metamorphic or magmatic event after the initial crystallization of the diorites and granodiorites at circa 3470 Ma. The North Shaw Suite (T94/193), part of the mylonitic granodiorite (T94/227), and the diorites (T94/222) crystallized between 3469 and 3463 Ma, whereas the predecessor of the gray gneisses (T94/221) crystallized at circa 3450 Ma, at the same time that new rims grew or that metamorphic recrystallization occurred. The U-Pb zircon results indicate that the diorites are older than the gray gneisses. The diorites may therefore have occurred as xenolithic boudins in the gray gneisses.

Activity on the SRSZ is constrained in time by the results from samples T94/193, T94/221 and T94/227 (Figure 3). The crystallization age of 3469±3 Ma obtained for T94/227 provides a maximum age for movement along the basal SRSZ, which formed the contact between the North Shaw Suite and the gray gneisses. The crystallization age of 3468±2 Ma determined for sample T94/193 confirms that the wedge of granodiorite in the southeastern Shaw Granitoid Complex is the continuation of the North Shaw Suite, consistent with a 3467±6 Ma age [*McNaughton et al.*, 1993] of the northern part of the complex. This date also provides a minimum age for the mylonitic fabric related to the SRSZ in the amphibolite greenstones, since the granodiorite has both intruded, and contains enclaves with, this fabric. Structural mapping [*Zegers et al.*, 1996, 1998] indicates that the mylonitic fabrics in the Shaw Granitoid Complex (SRSZ) and in the Coongan Belt (SGZS) are part of one geometric system: The two shear zones join toward the south and have identical kinematics. Although it is theoretically possible that the amphibolite grade mylonic fabrics in the granitoid rocks and greenstones are not one system, the geometric continuity and the kinematic consistency strongly suggest that these structures developed during a single synmagmatic structural event. Therefore the main episode of activity of this mylonite system, both in the Shaw Granitoid Complex and in the greenstones, is interpreted to have occurred at circa 3468 Ma. However, it is possible that the SRSZ, or part of its fabric, in the granitoid rocks is younger and may belong to a different structural event. Nevertheless, a minimum age for this event of 3222±13 Ma [*Zegers et al.*, 1998] was provided by the oldest $^{40}Ar/^{39}Ar$ cooling age obtained for hornblende from the SRSZ mylonite.

The gray gneisses, for which a crystallization age of 3451±1 Ma was determined, were observed to be truncated by the base of the SRSZ, indicating that the basal SRSZ must have been active or reactivated during or after 3451 Ma. Growth faults in the Coongan Belt are constrained by the age of the Duffer Formation at 3470±5 Ma [*Nelson*, 2001]. The Duffer Formation has been dated in other belts of the eastern Pilbara using conventional U-Pb zircon techniques, at 3471±3 Ma, 3465±3 Ma and 3470±2 Ma [*Thorpe et al.*, 1992], whereas felsic volcanics of the overlying

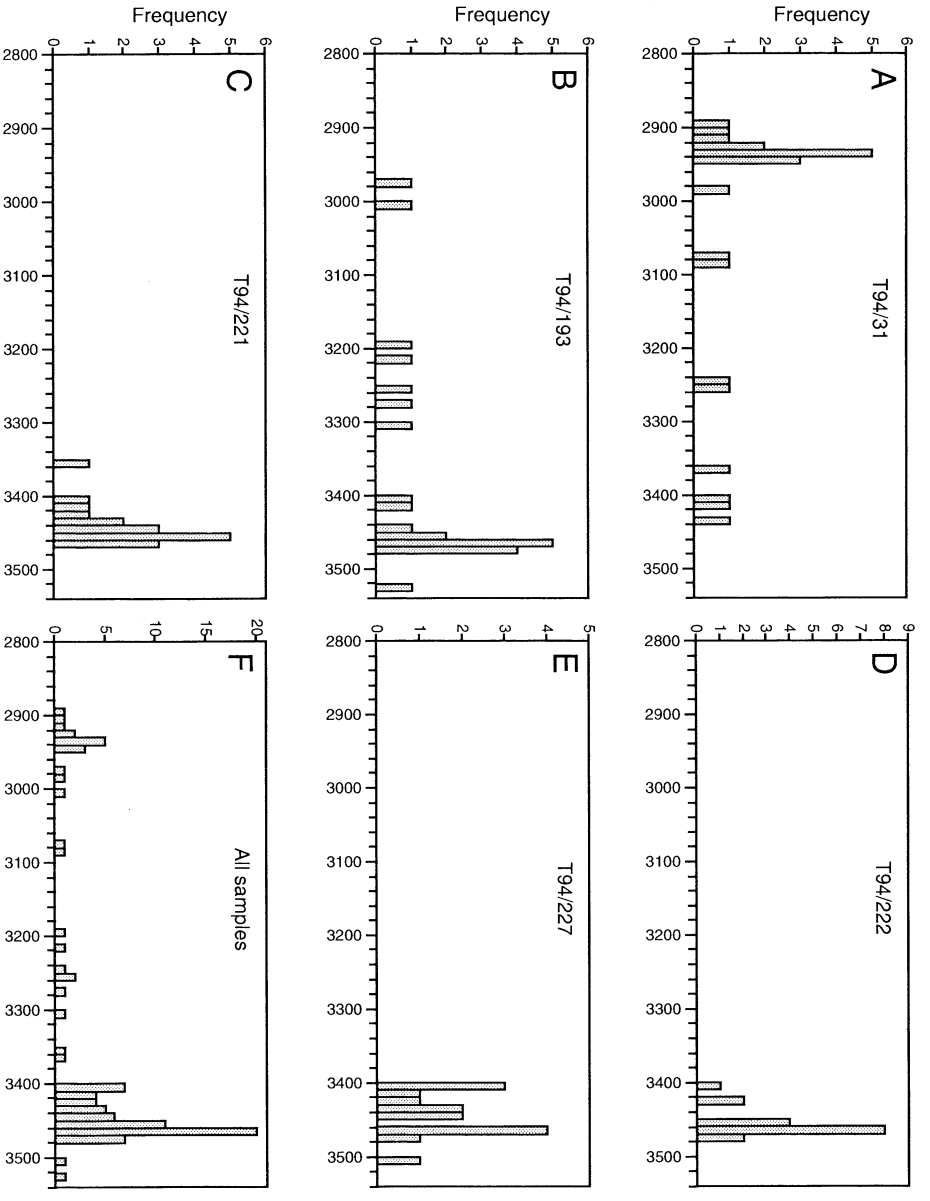

Figure 7. $^{207}Pb/^{206}Pb$ age histograms compiled from (a-e) the five samples that were analyzed and (f) of all analyzed spots combined. The age scale is in Ma and the histogram interval is 10 Ma. The data have been filtered using the following criteria: (1) analyses which were more than 15% discordant were omitted, and (2) analyses with more than 500 ppm U were omitted.

Salgash Subgroup have been dated at 3454±1 Ma [*Thorpe et al.*, 1992], the same age as the crystallization age of the precursor to the gray gneiss at 3451±1 Ma determined in this study. The gray migmatic gneisses and dioritic enclaves (3463±2 Ma) contain zircons with concordant ages as young as 3419 Ma, and T94/227, the mylonitic granodiorite, contains age groups of 3440±5 Ma and 3415±4 Ma. These zircon ages may represent the timing of high grade metamorphism and migmatization, after which the gray gneisses were unroofed by the SRSZ, implying that the SRSZ was active in an extensional environment until 3415 Ma.

Ages of circa 3300 Ma that occur in T94/31, T94/193 and T94/221 may reflect the influence of metamorphic disturbance events following initial activity of the SRSZ. It is possible that a part of the basal shear zone of the SRSZ was reactivated at this stage, for example during the 3.33-3.20 Ga brittle-ductile thrusting event identified within the Coongan Belt [*Zegers et al.*, 1999]. However the structures in the basal SRSZ lack any evidence, such as low temperature shear zones, for such later reactivation.

The ultramylonite in the MSZ is constrained in time by the crystallization age of the synkinematic granitic dyke (sample T94/31) at 2934±2 Ma. The granitic dyke has intruded an ultramylonitic part of the MSZ and contains the same mylonitic foliation and lineation as the MSZ. The dyke is thus synkinematic with development of the ultramylonite. Therefore the date of 2934 Ma obtained for the dyke constrains the time of movement on the north trending Mulgandinnah Lineament across the eastern Pilbara, of which the MSZ is part. However, the MSZ

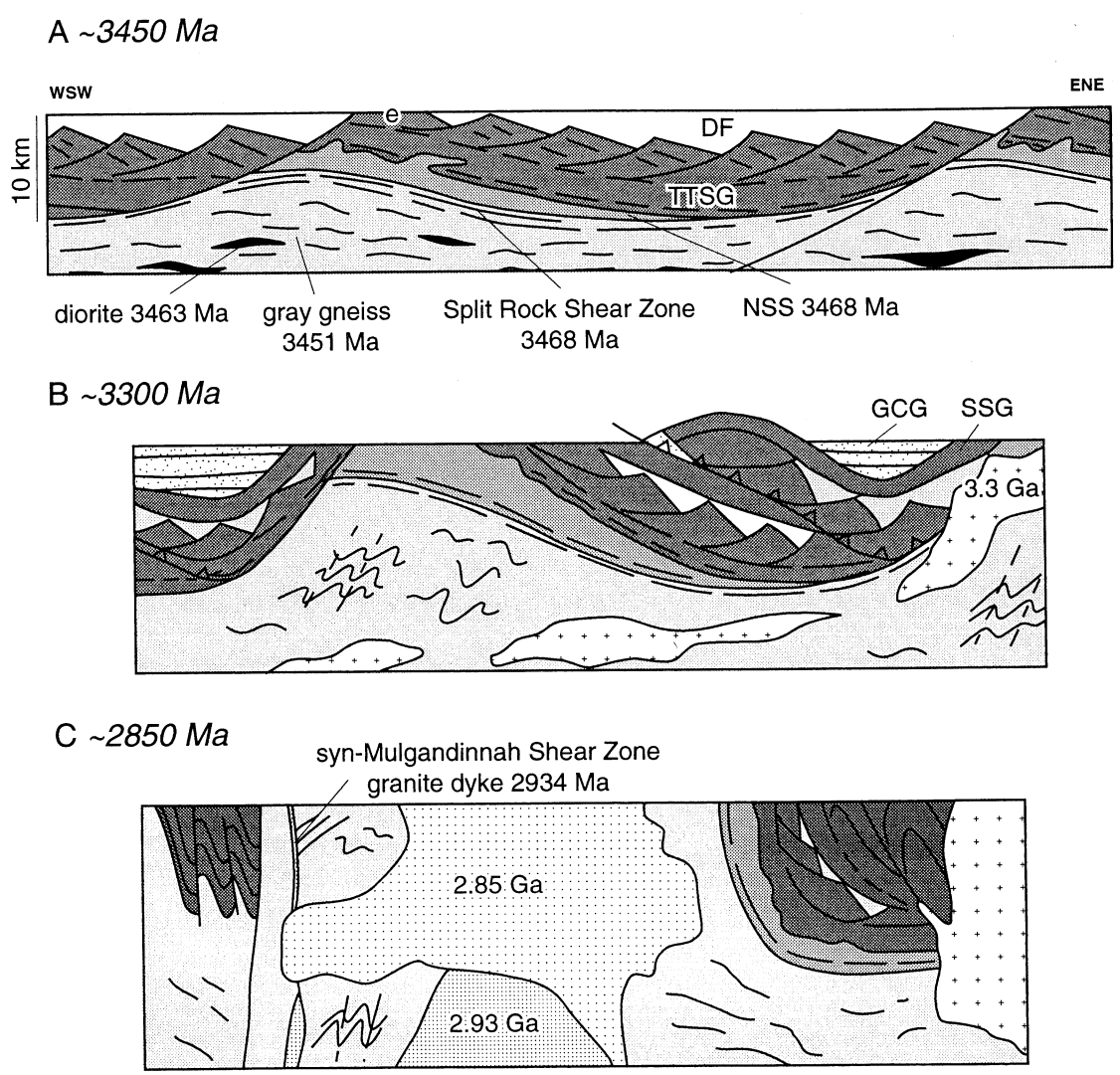

Figure 8. Schematic cross sections for different time frames through the Shaw Granitoid Complex and Coongan Belt (see Figure 1 for the approximate trace of the cross sections). Samples dated in this study are schematically shown in their structural position. (a) Extensional deformation between 3470 to 3420 Ma, resulting in a core complex type geometry with brittle faults in the upper crust and a detachment shear zone (Split Rock Shear Zone) at the midcrustal level. Basement to the extension was the Talga Talga Subgroup (TTSG)/Coonterunah Group, e indicates the area where erosion of the basement took place. Extension was active during intrusion of the North Shaw Suite (NSS) along the SRSZ and deposition of the felsic Duffer Formation (DF). Extension on the SRSZ resulted in the partial exhumation of gray migmatitic gneisses and granulitic diorites. (b) E-W compressional deformation after deposition of the Wyman Formation (WF), resulting in thrusting and folding of greenstone belt stratigraphy. SSG, Salgash Subgroup; GCG, Gorge Creek Group. (c) Pancratonic strike-slip deformation and synkinematic granite intrusion at 2.93 Ga; final postkinematic granite intrusion at 2.85 Ga; tilting of bedding and previously formed structures to generally steep orientations in the greenstone belts.

may have been active for a some time before synkinematic intrusion of the granitic dykes. $^{40}Ar/^{39}Ar$ cooling ages [*Zegers et al.*, 1999] indicate that the amphibolite grade fabric of the MSZ mylonite formed prior to 2944±9 Ma. The U-Pb zircon date of the granitic dyke is within error of this cooling age, indicating that the MSZ was active during cooling through the closure temperature of hornblende for argon.

5.2. Tectonothermal Development of the Shaw Granitoid Complex

SHRIMP U-Pb zircon dates from this and previous studies in the eastern Pilbara, including those obtained on xenocrystic and recrystallized zircons, are shown with $^{40}Ar/^{39}Ar$ cooling ages [*Davids et al.*, 1997; *Wijbrans and McDougall*, 1987; *Zegers et*

al., 1999] in Figure 2. Figure 2 shows that U-Pb dates in the Shaw area tend to record older crystallization events at circa 3520, 3470-3420, and 3330-3310 Ma, whereas the majority of the $^{40}Ar/^{39}Ar$ cooling ages record younger thermal events at 3250-3180 and Ma 3040-2850 Ma.

The new age constraints from this study may be used in combination with previous U-Pb and $^{40}Ar/^{39}Ar$ cooling ages to propose a tectonothermal history for the eastern Pilbara that is consistent with the geometric and kinematic development of the Shaw area. Figure 8 shows situation sketches of the geometry in cross section through the Shaw Granitoid Complex and the Coongan Belt, after each major tectonic and intrusive event identified.

5.2.1. Pre-3.5 Ga Basement. There is evidence to suggest that the 3515 Ma Coonterunah Group, described by *Buick et al.* [1995] from the Pilgangoora Greenstone Belt, was more extensive and also present in the Shaw area. This is indicated (Figure 2a) by three ages obtained for xenocrystic zircons from this study (3524± 6 and 3509±15 Ma) and from the Mount Edgar Granitoid Complex (3512±13 Ma [*Williams and Collins,* 1990]) and two $^{40}Ar/^{39}Ar$ hornblende cooling ages from the Talga Talga Subgroup in the Coongan Belt (3518±16 Ma [*Davids et al.,* 1997]) and in the greenstones adjacent to the northern part of the Shaw Granitoid Complex (3522±13 Ma [*Zegers et al.*, 1999]). The $^{40}Ar/^{39}Ar$ cooling ages from the lower Talga Talga Subgroup, for which the true age has so far remained elusive because of a lack of felsic lithologies suitable for dating, raise the possibility that the Coonterunah Group and parts of the Talga Talga Subgroup may be time equivalents, and possibly parts of the same sequence.

Basement to the extensional structures (discussed in the next section) is therefore inferred to be the 3515 Ma Coonterunah Group and parts of the Talga Talga Subgroup. The diorites and gray gneisses (3470-3450 Ma) in the core of the Shaw Granitoid Complex were formed during the extensional event and do not represent a deformed and metamorphosed basement to the extension. Bedding within the Talga Talga Subgroup units are subparallel or show a small angular unconformity, interpreted to be a result of growth fault tilting of the stratigraphy, with respect to the overlying Duffer Formation and Salgash Subgroup, and show the same low metamorphic grade. Therefore there is no evidence for a previous cycle of deformation and metamorphism in the mafic basement prior to deposition of the Duffer Formation.

The lower Talga Talga Subgroup has been likened to oceanic crust or an oceanic plateau [*Barley,* 1993; *Krapez,* 1993], but *Green et al.* [2000] have shown that volcanic rocks of the Coonterunah Group have crustal chemical signatures compared to N-MORB. In either case, the basement to the extensional event that commenced at 3470 Ma was a dominantly mafic and subaqueous volcanic sequence with oceanic geochemical affinties.

5.2.2. Interpretation of the 3.47-3.42 Ga extensional deformation event. An extensional event between 3470-3420 Ma has been identified (Figure 2a) in both granites and greenstones of the eastern part of the Pilbara Craton. This study has shown that emplacement of TTG magmas coincided with extensional deformation in both the brittle upper crust and the ductile lower crust. Age constraints on structures in the Shaw area may be used to reconstruct the geometry of the Shaw region during this extension episode (Figure 8). The Split Rock Shear Zone formed a detachment in the middle crust which is inferred to have been active from 3470 Ma to 3420 Ma. At 3470 Ma the diorite crystallized structurally below the SRSZ, while components of the North Shaw Granodiorite were intruded as sheets along the SRSZ (Figure 8).

A similar geometry for a synextensional granitoid intrusion has been described for the Basin and Range area [*Holm,* 1995; *Pavlis,* 1996], with deformation in sheeted granitoids concentrated at the base of the intrusion. Pavlis's thermomechanical modeling work indicates that intense fabric development at the base of the granitoid sheet is typical during intrusion within an extensional environment. This is consistent with our interpretation that the North Shaw Suite was intruded and deformed in an extensional environment.

Extension on the SRSZ continued or may have been reactivated at or after 3450 Ma, when large-scale melting of the lower crust resulted in emplacement of the precursor of the gray gneisses at 3450 Ma. The gneiss and diorite were subsequently deformed, metamorphosed, and migmatized, at circa 3420 Ma, then partly exhumed and truncated by the SRSZ.

The domal shape of the Shaw Granitoid Complex must have at least partly developed during this early deformation event by a combination of extensional core complex formation and emplacement of sheet-like intrusions of granodiorite. Brittle extensional structures formed contemporaneously [*Zegers et al.,* 1996] in the upper lithosphere in the Talga Talga Subgroup during extrusion of the Duffer Formation. This may have resulted in a fault-related topography in which some domed areas were eroded ("e" in Figure 8). This erosional unconformity between the Talga Talga Subgroup and the overlying Salgash Subgroup may be represented by the angular unconformity in the Pilgangoora Belt described by *Buick et al.* [1995]. In the Coongan Belt the extensional faults were filled by felsic volcanics and clastic sediments of the Duffer Formation followed by deposition of the Salgash Subgroup.

Brittle faults, similar to those in the Coongan Belt, have been identified throughout a large area of the eastern Pilbara between the Kelly Belt and Mulgandinnah Shear Zone [*Nijman et al.,* 1998], but the directions of transport are not well established. Recent SHRIMP U-Pb zircon dating has shown that the Carlindi [*Buick et al.,* 1995], Muccan [*Nelson,* 1996] and Yule Granitoid Complexes [*Nelson,* 1999] contain important 3470-3420 Ma TTG components, similar to the Shaw and the Mount Edgar Granitoid Complexes (Figure 2). Therefore this magmatic event, associated with extension, occurred in the Yule, Carlindi, Muccan, Mount Edgar, Corunna Downs, and Shaw Granitoid Complexes (150 x 200 km). If extension and TTG magmatism were genetically related as argued here, this observation suggests that a large proportion of the eastern part of the Pilbara Craton was subjected to extensional deformation between 3460 and 3450 Ma.

5.2.3. Compressional deformation at 3.33-3.2 Ga. The first major tectonic event after the 3.47-3.42 Ga extension episode, and following at least 100 Ma of quiescence, that can be recognized in the Shaw area, is an E-W compression event. In the Coongan Belt, this event is constrained to between 3315 Ma, the age of the Wyman Formation which is deformed by thrusts, and 3.2 Ga, the $^{40}Ar/^{39}Ar$ cooling age of postkinematic actinolites [*Zegers et al.,* 1999] (Figure 2). Structures that belong to this phase have been described in the Tambourah [*Boulter et al.,* 1987], Warrawoona [*Kloppenburg et al.,* 2001], Marble Bar [*van Haaften and White,* 1998] and the Coppins Gap belts [*Nijman et al.*, 1998]. In the greenstone belts the thrusts have caused repetition of the stratigraphy and thrust-related folding (Figure 8b).

Although the granitic domes formed during extension, it is likely that the domal geometry was enhanced during the

compression event. The N-S trending sections (i.e. the eastern margin of the Shaw Granitoid Complex) were probably steepened to some extent during E-W compression. However, as discussed further below, steepening of bedding and structures also occurred at a later stage.

5.2.4. Strike-slip deformation at 2.93 Ga. *Krapez* [1993] subdivided the Pilbara Craton into five domains separated by craton-scale sinistral NNE trending strike-slip lineaments (Figure 1). These domains were considered to have been active during deposition of clastic sediments within several depositional basins at circa 2950 Ma. This study has shown that one of these lineaments, the Mulgandinnah Shear Zone, was active at 2934 Ma. Granites were intruded at 2.93 Ga into the Mulgandinnah Shear Zone and were deformed, but movement within this shear zone postdated the gneissic foliations and mylonites that were related to the SRSZ (Figure 3). The geochronology data summarized in Figure 2 indicate that there were three intervals of granite intrusion, at circa 3.0 Ga, 2.93 Ga and 2.85 Ga. The 2.85 Ga granite has truncated, and therefore its intrusion postdates activity within the MSZ.

The only other pancratonic shear zone in the Pilbara that has been studied to some extent is the Sholl Shear Zone (Figure 1). *Smith et al.* [1998] showed that dextral movement occurred on the E-W trending part of this shear zone [*Zegers,* 1996] at circa 2960 Ma. If the Pilbara granite-greenstone terrain was one continental block at 2.95 Ga, the north trending sinistral MSZ and the east trending dextral Sholl Shear Zone can be interpreted as two conjugate shears in a NW-SE directed compressional stress field.

5.2.5. Steepening of bedding and structures. One of the conspicuous features of the eastern part of the Pilbara Craton is that on a regional scale, structures and bedding in greenstones have steep, partly synclinal geometries that wrap around the granitoid domes (Figure 1). Dips are generally shallow (20°-40°) close to or in the roof of granitoid complexes (Marble Bar Belt, North Pole area) and steepen or are sometimes overturned further away from the granitoid complexes (e.g., in the Coongan and Coppin Gap belts).

Tilting must have occurred late in the development of the eastern part of the Pilbara Craton, largely after the 3460 Ma extensional, and 3.3-3.2 Ga compressional phase. Late tilting is indicated by the steep orientation of the youngest stratigraphic units in the greenstone belts, such as the clastic metasedimentary rocks which have been correlated with the Lalla Rookh Sandstone. The angular unconformity between these sediments and older volcanic units is usually minor, typically 20°-30° (see, for examples, north Coongan Belt, Figure 3, and for the Coppin Gap Belt, *Nijman et al.,* [1998]). Recent SHRIMP U-Pb zircon dating of detrital zircons from a metasandstone taken from the Lalla Rookh basin [*Nelson,* 2001] has indicated a maximum age of deposition of 3304 ± 6 Ma for the sandstone. No zircons younger than this age were detected in this sandstone, suggesting that the Lalla Rookh basin may be much older than its assumed 2950 Ma age. This interpretation constrains the timing of at least the major component of the tilting to later than c. 3.3 Ga.

5.3. Tectonic Regimes in the Mid-Archean

The results from this study can be used to speculate on possible tectonic regimes in the Archean. Models for the evolution of Archean granite-greenstone terrains are currently of two general types:

1. Tectonic processes in the Archean were similar to present day [*Burke et al.,* 1976], including subduction and accretion of volcanic arcs, back arcs, and oceanic plateaus accreted in a Turkic-type orogeny [*Sengör and Natal'in,* 1996]. However, the higher radioactive heat production in the Archean has important consequences. To dissipate that amount of heat through plate tectonic processes, the rate of production of oceanic crust must have been faster, resulting in either faster spreading and/or smaller plates [*Sleep and Windley,* 1982]. Arguments based on the geochemistry of the volcanic rocks [*Barley,* 1993] and greenstone stratigraphy [*Krapez,* 1993] have been used in support of this type of model for the Pilbara.

2. The Archean Earth was too hot to allow present day style plate tectonics to occur. Heat was dissipated through mantle plumes and (solid state) diapiric processes in the continental crust. *Choukroune et al.* [1995] proposed that a diapiric Earth was operating in the early to Mid Archean, changing to interaction of lithospheric plates toward the Late Archean. Diapiric models have been proposed for the eastern part of the Pilbara Craton [*Hickman,* 1984] and for the Mt. Edgar Granitoid Complex, in particular [*Collins,* 1989; *Collins et al.,* 1998].

Analysis of unconformities and bedding orientations that define the doming pattern in the eastern Pilbara shows that the main component of doming occurred following deposition of the upper clastic sequences with a maximum depositional age of 3304±6 Ma. Therefore, if diapirism did play a role in the development of this terrane, it must have ocurred late in the evolution, possibly during intrusion of 3.0 to 2.85 Ga granites. Diapirism as the result of a mantle plume at 3.325 Ga [*Collins et al.,* 1998] is inconsistent with the timing of doming. The lack of major mafic and ultramafic sequences in the younger stratigraphic units does not favor a connection between doming and mantle plume activity.

The post 3.3 Ga development of the Pilbara craton can largely be explained by compressional interaction between lithospheric plates. The 3.3 to 3.2 Ga compressional structures are found regionally (i.e., in an area larger than one belt) and with a uniform compressional direction (E-W) [*Boulter et al.,* 1987; *Nijman et al.,* 1998; *van Haaften and White,* 1998; *Zegers et al.,* 1996]. Externally applied plate tectonic stresses are therefore required at circa 3.2 Ga. Figure 2 shows that the first joint magmatic event in the east and west Pilbara occurs at circa 3.25 Ga, i.e., possibly during the compressional event. The E-W compression in the Shaw area may therefore be the result of the accretion of existing parts of the western Pilbara to an eastern Pilbara nucleus. A suture between the east and west Pilbara may be located beneath the Mallina Basin (Figure 1).

Rigid lithospheric plates are a prerequisite for strike-slip systems of the size of the Mulgandinnah Shear Zone (200 km long) to form [*Sleep,* 1992]. Therefore, by 2.95 Ga the continental crust of the Pilbara Craton must have had rheological properties similar to those of the present day continental crust.

Although the tectonic development after 3.3 Ga is consistent with interaction of rigid lithospheric plates, the evidence is still insufficient to accept present day plate tectonics, including accretion and subduction of terranes originating in various tectonic settings, as the model for the entire evolution of the Pilbara Craton between 3.3 and 2.8 Ga. Independent elements of the geology of the eastern Pilbara, such as thrusting, folding and calc-alkaline trends of some magmatic rocks, may be interpreted in terms of present-day tectonic processes, but the complete association of stratigraphy, magmatism, metamorphism, structures, and especially their timing, are difficult to fit into one or several orogenic cycles incorporating arcs and oceanic plateaus.

The 3470-3420 Ma TTG–extensional event in the Shaw area cannot readily be interpreted in terms of modern-day plate tectonic processes. The key elements of this event are extension of a relatively undeformed mafic volcanic basement, coeval with TTG melt intrusion and high-temperature metamorphism. TTG melts have been regarded as slab melts in a subduction zone, similar to modern day adakites [*Martin,* 1999]. However, in a comparison between Archean TTG's and modern arc-related adakites, *Smithies* [2000] showed that the pre-3.4 Ga TTGs in the Pilbara are not consistent with formation by slab melt in a subduction setting, because they lack a mantle wedge signature. The mid-Archean TTGs are more consistent with melting of the base of the mafic crust.

In addition, characteristics of an arc setting, such as a linear distribution of rocks units and structures, high-pressure metamorphism, paired metamorphic belts, melange zones, and turbidite sequences, have not been identified in the pre-3.4 Ga rock record of the Pilbara Craton. Although extension is commonly a feature of volcanic arcs, Archean subduction zones are expected to have been shallow [*Vlaar et al.,* 1994; *Hoffmann,* 1997], leading to a compressional arc with dominant thick skinned deformation [*Jordan et al.,* 1983], and not to extension as occurred in the Pilbara during the 3470-3420 Ma event. An arc setting for the TTG-extension event is therefore inconsistent with these geological observations.

The arrival of a plume head under existing continental or oceanic crust may lead to doming and extension. Such a model has been proposed for the Late Archean Yilgarn Craton [*Campbell and Hill,* 1988; *Hill,* 1991]. In such a model, extension is expected to coincide with voluminous mafic and ultramafic volcanism, with this followed by generation of late stage minor crustal melts. In the case of oceanic crust, TTG melts may be generated. However, the large volume of the 3470-3420 Ma TTG melt in the Pilbara, and the coincidence of extension with TTG intrusion, is difficult to reconcile with a mantle plume type-model.

A model that may be consistent with many observations of the TTG-extension event is delamination or convective thinning of the lower part of a thick oceanic crust or oceanic plateau, as a consequence of eclogitization of the lower crust [*Davies,* 1992; *Vlaar et al.,* 1994]. Delamination may result in uplift, extension, and disturbance of the geotherm, resulting in high-temperature metamorphism and melting of the lower crust [*Kay and Kay,* 1993]. This is consistent with the main elements of the 3470-3420 Ma event in the Pilbara granite-greenstone terrain.

6. Conclusions

SHRIMP U-Pb zircon data obtained in this study show that extension in the upper (brittle listric faults) and middle crust (extensional detachment) was synchronous, and was associated with volumetrically extensive intrusion of TTG granitoids and the extrusion of felsic and (ultra) mafic volcanics between 3480 and 3420 Ma. High-temperature metamorphism and migmatization of gray gneisses and diorites, with crystallization ages of 3451±1 and 3463±3 Ma, respectively, probably occurred at circa 3420 Ma, after which they were exhumed by the extensional SRSZ. The mafic oceanic plateaux like Talga Talga Subgroup and Coonterunah Group provided the "basement" to this extensional deformation. This combined extensional and TTG magmatic event is difficult to reconcile with either modern-day subduction-related or mantle plume-related tectonic settings, but aspects of the geological development of the Pilbara craton at this time are consistent with a model involving delamination of part of the lithosphere.

Pancratonic sinistral strike-slip deformation on the north trending Mulgandinnah Shear Zone occurred at 2.93 Ga. This is roughly synchronous with dextral strike-slip on the east trending Sholl Shear Zone in the western Pilbara (2.96 Ga) [*Smith et al.,* 1998]. Both are consistent with a NW-SE directed regional stress field at this stage.

Deformation related directly to granite diapirism did not play a major role in the 3.5-3.3 Ga evolution of the Shaw area. Steepening of bedding and doming is a post 3.3 Ga feature that may be related to the extraction of granitic melt from the lower crust and intrusion in the upper crust between 3.0 and 2.85 Ga.

Structural development of the eastern part of the Pilbara Craton from circa 3.3 Ga is consistent with the interaction of rigid lithospheric plates that were capable of transmitting far-field stresses, resulting in E-W directed compression and later pancratonic strike-slip zones. Evidence of the involvement of present day style tectonic processes, including subduction, remains equivocal for this period.

Appendix A

A1. Sample Preparation

The zircon separation and sample preparation were done in the mineral separation laboratory at Vrije University in Amsterdam. Rock samples with a weight of ~10 kg were crushed and ground to a particle size smaller than 500 μm and subsequently sieved in fractions larger and smaller than 250 μm. The zircons were separated from the latter by successively (1) removing particles smaller than 32 μm, by sieving in water, (2) removing the light quartz-feldspar fraction with a large overflow centrifuge (LOC-500) developed at the Vrije University using a sodium polytungstate solution (d = 2.8 g/cm^3), (3) removing magnetic ores with an ore magnet and subsequently separating magnetic fractions with a Carpco magnet separator, (4) density separation to remove minerals such as hornblende from the denser fraction, with a laboratory overflow centrifuge (LOC-50) with di-iodomethane (d= 3.28 g/cm^3).

The heavy fraction was then sieved into size fractions (<30 μm, 30-60 μm, 60-90 μm, and 90-120 μm), using anisotropic sieves with oblong holes, whereby crystals are separated based on their width. These fractions were further separated using a Frantz isodynamic magnetic separator. The final zircon separation was done by handpicking ~50-150 clear, preferably whole grains for each sample. During the mineral separation procedure, particular care was taken to avoid sample cross contamination. The selected zircons were mounted in epoxy and sectioned approximately in half. The mount surface was then polished to expose the grain interiors. All zircons were then photographed in transmitted and reflected light under a microscope. Cathodoluminescence images were made on the scanning electron microscope (XL-30) of the larger grains.

A2. Analytical Methods

U-Th - Pb measurements were made using the ion microprobe SHRIMP II at Curtin University of Technology, employing the operating and data processing procedures similar to those described by [*Compston et al.,* 1984] and [*Williams et al.,* 1984]. Pb/U ratios were determined relative to that of the standard Sri Lankan zircon CZ-3, which has been assigned a $^{206}Pb/^{238}U$ value of 0.0914 corresponding to an age of 564 Ma.

Reproducibility of the Pb/U ratio of the standard was in most cases better than ±3.0%. Where this was not the case for part of the session, the standards were grouped separately so that the

reproducibility per group was better than 3%. One of the standard measurements was treated as an outlier and was not used in the data reduction procedure. This uncertainty is included in the quoted analytical errors. Errors given on individual analyses are based on counting statistics and are at the 1 σ level; those given on pooled analyses are at t (where t is Fisher's t) or 95% confidence. Error boxes shown in the Figures are at the 1 σ level.

The processing of the raw data and plotting on conventional concordia plots was undertaken using computer software written by D.R. Nelson. Experience with the Perth Consortium SHRIMP II confirms that the relationship between Pb/U and UO/U is best described by a power law. This relationship has been incorporated into the data reduction procedures. Similar and generally low ^{204}Pb counts were measured on both standards and unknown samples and common-Pb corrections have therefore been applied using the measured ^{204}Pb abundance and assuming the isotopic composition of Broken Hill common-Pb, as this is the composition of ambient lead in the environment. Where this is inapplicable (see Table 2), common-Pb compositions have been determined using the model of *Cumming and Richards* [1975]. In general terms, Cumming and Richards' common Pb compositions have been assumed when the measured ^{204}Pb counts (less those measured at the baseline at mass 204.1) on the unknowns are more than 6 times the average ^{204}Pb counts (less those measured at the baseline at mass 204.1) measured on the standards during the analyses session. Corrections for ^{206}Pb hydride isobaric interference at ^{207}Pb and excess ^{204}Pb counts (commonly observed during measurements on the Australian National University SHRIMP-1) were not required for any of the samples reported here.

The samples investigated in this study were granitic in nature, and the zircon populations recovered from most samples were dominated by a single morphological type. Features such as zircon morphology (size, shape, zonation, etc.) and chemistry (U and Th contents, Th/U ratios), degree of discordance of each analyses, and evidence of radiogenic Pb loss were taken into account in the assessment of the validity of pooled analyses.

Analyses obtained for the majority of samples were either concordant or defined radiogenic Pb loss trajectories indicating recent Pb loss. Dates were therefore determined using the mean $^{207}Pb/^{206}Pb$ ratios determined from pooled analyses. Individual analyses were weighted according to the inverse square of the individual analytical error (based on counting statistics) of the analyses, for the determination of the mean $^{207}Pb/^{206}Pb$ ratio of pooled analyses. Analyses more than ±2 σ from the weighted mean value were treated as outliers and deleted from the pool, and the weighted mean value then recalculated. This process was repeated until all pooled analyses were all within ±2 σ of the weighted mean value, and the remaining pooled data were normally distributed about the mean. A chi^2 test was applied to grouped analyses in order to assess the relative effects of analytical sources of error, such as counting statistics and uncertainty in the common Pb composition, and geological sources of error, such as that arising from the inclusion of analyses of slightly older xenocryst zircons or of analyses that may have lost small amounts of radiogenic Pb during ancient disturbances. Chi^2 values for grouped analyses of less than or equal to unity indicate that scatter about the weighted mean value determined for the grouped analyses can be accounted for by analytical sources of error alone. A chi-square value significantly greater than unity indicates that analyses are not normally distributed about the weighted mean value and that other (geological) sources of error are present within the grouped population. In these cases, the 95% confidence error is based on the observed scatter about the weighted mean $^{207}Pb/^{206}Pb$ ratio of pooled analyses.

Acknowledgments. Financial support of the Dr. Schürmann Foundation for Precambrian Research for fieldwork is acknowledged (grants 1993/05 and 1994/09). T.Z. acknowledges field assistance from Jan Kees Blom. Timon Fliervoet and Martin Drury helped with the CL images of the zircons. The mineral separation would not have been possible without the help of Lodewijk Ijlst. Comments on earlier drafts of the manuscript by Armelle Kloppenburg and Jan Kees Blom are much appreciated. We thank Denis O'Meara for hospitality in Marble Bar. D.R.N. publishes with the permission of the Director, GSWA.

References

Barley, M.E., Volcanic, sedimentary and tectonostratigraphic environments of the ~3.46 Ga Warrawoona Megasequence: A review, *Precambrian Res., 60*, 47-67, 1993.

Barley, M.E., and A.L. Pickard, An extensive, crustally-derived, 3325 to 3310 Ma silicic volcanoplutonic suite in the eastern Pilbara Craton: Evidence from the Kelly Belt, McPhee Dome and Corunna Downs Batholith, *Precambrian Res., 96*, 41-62, 1999.

Barley, M.E., S.E. Loader, and N.J. McNaughton, 3430 to 3417 Ma calc-alkaline volcanism in the McPhee Dome and Kelly Belt, and growth of the eastern Pilbara Craton, *Precambrian Res., 88*, 3-24, 1998.

Bickle, M.J., L.F. Bettenay, M.E. Barley, H.J. Chapman, D.I. Groves, I.H. Campbell, and J.R. de Laeter, A 3500 Ma Plutonic and volcanic calc-alkaline province in the Archean east Pilbara Block, *Contrib. Mineral. Petrol., 84*, 25-35, 1983.

Bickle, M.J., P. Morant, L.F. Bettenay, C.A. Boulter, T.S. Blake, and D.I. Groves, Archean tectonics of the Shaw Batholith, Pilbara block Western Australia: Structural and metamorphic tests of the batholith concept., *Geol. Assoc. Can. Spec. Pap., 28*, 325-341, 1985.

Bickle, M.J., L.F. Bettenay, H.J. Chapman, D.I. Groves, N.J. McNaughton, I.H. Campbell, and J.R. de Laeter, The age and origin of younger granitic plutons of the Shaw Batholith in the Archean Pilbara block, Western Australia, *Contrib. Mineral. Petrol., 101*, 361-376, 1989.

Boulter, C.A., M.J. Bickle, B. Gibson, and R.K. Wright, Horizontal tectonics pre-dating upper Gorge Creek sedimentation Pilbara Block, Western Australia, *Precambrian Res., 36*, 241-258, 1987.

Buick, R., J.R. Thornett, N.J. McNaughton, J.B. Smith, M.E. Barley, and M. Savage, Record of emergent continental crust ~3.5 billion years ago in the Pilbara Craton of Australia, *Nature, 375*, 574-577, 1995.

Burke, K.C.A., J.F. Dewey, and W.S.F. Kidd, Dominance of horizontal movements, arc and microcontinental collisions during the later permobile regime, in *The Early History of the Earth*, edited by B.F. Windley, pp. 113-129, John Wiley, New York, 1976.

Campbell, I.H., and R.I. Hill, A two-stage model for the formation of the granite-greenstone terrains of the Kalgoorlie-Norseman area, Western Australia., *Earth Planet. Sci. Lett., 90*, 11-25, 1988.

Choukroune, P., H. Bouhallier, and N.T. Arndt, Soft lithosphere during periods of Archean crustal growth or crustal reworking, in *Early Precambrian Processes*, vol. 95, edited by M.P. Coward and A.C. Ries, *Geol. Soc. L. Spec. Publ., 95*, 67-86, 1995.

Collins, W.J., Polydiapirism of the Archean Mount Edgar Batholith, Pilbara Block, Western Australia, *Precambrian Res., 43*, 41-62, 1989.

Collins, W.J., M.J. van Kranendonk, and C. Teyssier, Partial convective overturn of Archean crust in the east Pilbara Craton, Western Australia: Driving mechanisms and tectonic implications, *J. Struct. Geol., 20*, 1405-1424, 1998.

Compston, W., I.S. Williams, and C. Meyer, U-Pb geochronology of zircons from lunar breccia 73217 using a sensitive high mass-resolution ion microprobe, *J. Geophys. Res., 89*, B252-B534, 1984.

Cooper, J.A., P.R. James, and R.W.R. Rutland, Isotopic dating and structural relationships of granitoids and greenstones in the East Pilbara, Western Australia, *Precambrian Res., 18*, 199-236, 1982.

Cumming, G.L., and J.R. Richards, Ore lead isotope ratios in a continuously changing earth, *Earth Planet. Sci.Lett., 28*, 155-171, 1975.

Davids, C., J.R. Wijbrans, and S.H. White, $^{40}Ar/^{39}Ar$ laserprobe ages of metamorphic hornblendes from the Coongan Belt, Pilbara, western Australia, *Precambrian Res., 83*, 221-242, 1997.

Davies, G.F., On the emergence of plate tectonics, *Geology*, 20, 963-966, 1992.

de Ronde, C.E.J., and M.J. de Wit, Tectonic history of the Barberton Greenstone Belt, South Africa: 490

million years of Archean evolution, *Tectonics, 13*, 983-1005, 1994.

Green, M.G., P.J. Sylvester, and R. Buick, Growth and recycling of early Archaean continental crust: Geochemical evidence from the Coonterunah and Warrawoona Groups, Pilbara Craton, Australia, *Tectonophysics, 322*, 69-88, 2000.

Hickman, A.H., Archean diapirism in the Pilbara, in *Precambrian Tectonics Illustrated*, edited by A. Kröner and R. Greiling, pp. 113-128, Nagele und Obermiller, Stuttgart, Germany, 1984.

Hill, R.I., Starting plumes and continental break-up, *Earth Planet. Sci. Lett., 104*, 389-416, 1991.

Hofmann, A.W., Early evolution of continents, *Science*, 275, 498-499, 1997.

Holm, D.K., Relation of deformation and multiple intrusion in the Death Valley extended region, California, with implications for magma entrapment mechanism, *J. Geophys. Res., 100*, 10,495-10,505, 1995.

Jordan, T., B. Isacks, R.W. Allmendinger, J.A. Brewer, V.A. Ramos, and C.J. Ando, Andean tectonics related to geometry of subducted Nazca plate, *Geol. Soc. Am. Bull., 94*, 341-361, 1983.

Kay, R.W., and S.M. Kay, Delamination and delamination magmatism, *Tectonophysics, 219*, 177-189, 1993.

Kloppenburg, A., S.H. White, and T.E. Zegers, The role of mid-crustal detachments in the non-diapiric development of the Pilbara Craton, Australia, *Precambrian Res.*, in press, 2001.

Krapez, B., Sequence statigraphy of the Archean supracrustal belts of the Pilbara Block, Western Australia, *Precambrian Res., 60*, 1-45, 1993.

Krapez, B., and M.E. Barley, Archean strike-slip faulting and related ensialic basins: Evidence from the Pilbara Block, Australia, *Geol. Mag., 124*, 555-567, 1987.

Lowe, D.R., Restricted shallow-water sedimentation of early Archean stromatolitic and evaporitic strata of the Strelley pool chert, Pilbara block, Western Australia, *Precambrian Res., 19*, 239-83, 1983.

Martin, H., Adakitic magmas: Modern analogues of Archaean granitoids, *Lithos*, 46, 411-429, 1999.

McNaughton, N.J., W. Compston, and M.E. Barley, Constraints on the age of the Warrawoona Group, eastern Pilbara Block, Western Australia, *Precambrian Res., 60*, 69-98, 1993.

Nelson, D.R., Compilation of SHRIMP U-Pb zircon geochronology data, 1995, Geol Surv. of West. Aust., record 1996/2, Perth, 1996.

Nelson, D.R., Compilation of SHRIMP U-Pb zircon geochronology data, 1996, Geol. Surv. of West. Aust., record 1997/2, Perth, 1997a.

Nelson, D.R., Evolution of the Archean granite-greenstone terranes of the Eastern Goldfields, Western Australia: SHRIMP U-Pb zircon constraints, *Precambrian Res., 83*, 57-81, 1997b.

Nelson, D.R., Compilation of SHRIMP U-Pb zircon geochronology data, 1997 Geol. Surv. of West. Aust., record 1998/2 Perth, 1998.

Nelson, D.R., Compilation of SHRIMP U-Pb zircon geochronology data, 1998, Geological Survey of Western Australia Geol. Surv. of West. Aust., record 1999/2, Perth, 1999,

Nelson, D.R., Compilation of SHRIMP U-Pb zircon geochronology data, 1999, Geol. Surv. of West. Aust., record 2000/2, Perth, 2000.

Nelson, D.R., 2001, Compilation of SHRIMP U-Pb zircon geochronology data, 1999, Geol. Surv. of West. Aust., record 2001/2, Perth, 2001.

Nijman, W., B.A. Willigers, and A. Krikke, Tensile and compressive growth structures: Relationship between sedimentation, deformation and granite intrusion in the Coppin Gap Greenstone Belt, eastern Pilbara, Western Australia, *Precambrian Res., 88*, 83-108, 1998.

Pavlis, T.L., Fabric development in syn-tectonic intrusive sheets as a consequence of melt-dominated flow and thermal softening of the crust, *Tectonophysics, 253*, 1-31, 1996.

Pidgeon, R.T., 3450 Ma old volcanics in the Archean layered greenstone succession in the Pilbara Block, Western Australia, *Earth Planet. Sci. Lett., 37*, 421-428, 1978a.

Pidgeon, R.T., Geochronological investigation of granite batholiths of the Archean granite-greenstone terrain of the Pilbara Block, Western Australia, in *Proceedings of 1978 Archean Geochemistry Conference*, edited by E.M. Smith and J.G. Williams, pp. 360-362, University of Toronto, 1978b.

Pidgeon, R.T., Recrystallization of oscillatory zoned zircon: some geochronological and petrological implications, *Contrib. Mineral. Petrol., 110*, 463-472, 1992.

Polat, A., R. Kerrich, and D.A. Wyman, The late Archean Schreiber-Hemlo and White River-Dayohessarah greenstone belts, Superior Province: Collages of oceanic plateaus, oceanic arcs, and subduction complexes, *Tectonophysics, 289*, 295-326, 1998.

Puchel, I.S., A.W. Hofmann, K. Mezger, K.P. Jochum, A.A. Shchipansky, and A.V. Samsonov, Oceanic plateau model for continental crustal growth in the Archean: A case study from the Kostomuksha greenstone belt, NW Baltic Shield, *Earth Planet. Sci. Lett, 155*, 57-74, 1998.

Sengör, A.M.C., and B.A. Natal'in, Turkic-type orogeny and its role in the making of the continental crust, *Annu. Rev. Earth Planet. Sci., 24*, 263-337, 1996.

Sleep, N.H., Archean plate tectonics: What can be learned from continental geology?, *Can. J. Earth Sci., 29*, 2066-2071, 1992.

Sleep, N.H., and B.F. Windley, Archean plate tectonics: constraints and inferences, *J.Geol., 90*, 363-379, 1982.

Smith, J.B., M.E. Barley, D.I. Groves, B. Krapez, N.J. McNaughton, M.J. Bickle, and H.J. Chapman, The Sholl Shear Zone, Western Pilbara: Evidence for a domain boundary structure from integrated tectonostratigraphic analyses, SHRIMP U-Pb dating and isotopic and geochemical data of granitoids, *Precambrian Res., 88*, 1998.

Smithies, R.H., The Archaean tonalite-trondhjemite-granodiorite (TTG) series is not an analogue of Cenozoic adakite, *Earth Planet. Sci. Lett., 182*, 115-125, 2000.

Thorpe, R.I., A.H. Hickman, D.W. Davis, J.K. Mortensen, and A.F. Trendall, U-Pb zircon geochronology of Archean felsic units in the Marble Bar region, Pilbara Craton, Western Australia, *Precambrian Res., 56*, 169-189, 1992.

van Haaften, M.W., and S.H. White, Evidence for multiphase deformation in the Archean basal Warrawoona Group in the Marble bar area, eastern Pilbara, western Australia, *Precambrian Res., 88*, 52-66, 1998.

van Kranendonk, M.J., and W.J. Collins, Timing and tectonic significance of Late Archean, sinistral strike-slip deformation of the Central Pilbara Corridor, Pilbara Craton, Western Australia, *Precambrian Res., 88*, 207-232, 1998.

Vlaar, N.J., P.E. van Keken, and A.P. van den Berg, Cooling of the Earth in the Archean: Consequences of pressure-release melting in a hotter mantle, *Earth Planet. Sci. Lett., 121*, 1-18, 1994.

Wijbrans, J.R., and I. McDougall, On the metamorphic history of an Archean granitoid greenstone terrane, East Pilbara, Western Australia, using the $^{40}Ar/^{39}Ar$ age spectrum technique, *Earth Planet. Sci. Lett., 84*, 226-242, 1987.

Williams, I.S., and W.J. Collins, Granite-greenstone terranes in the Pilbara Block, Australia, as coeval volcano-plutonic complexes: Evidence from U-Pb zircon dating of the Mount Edgar Batholith, *Earth Planet. Sci. Lett., 97*, 41-53, 1990.

Williams, I.S., R.W. Page, D. Froude, J.J. Foster, and W. Compston, Early crustal components in the Western Australian Archean: Zircon U-Pb ages by ion microprobe analysis from the Shaw Batholith and Narryer metamorphic belt, paper presented at the Sixth Australian Geological Convention, Lithosphere Dynamics and Evolution of Continental Crust, Geol. Soc. Aust., Canberra, ACT, Australia, 1983.

Williams, I.S., W. Compston, L.P. Black, T.R. Ireland, and J.J. Foster, Unsupported radiogenic Pb in zircon: A cause of anomalously high Pb-Pb, U-Pb and Th-Pb ages, *Contrib. Mineral. Petrol., 88*, 322-327, 1984.

Zegers, T.E., Structural, kinematic and metallogenic evolution of selected domains of the Pilbara granitoid-greenstone terrain: Implications for Mid Archean tectonic regimes, Ph.D. thesis, Utrecht Univ., Netherlands, 1996.

Zegers, T.E., S.H. White, M. de Keijzer, and P. Dirks, Extensional structures during deposition of the 3460 Ma Warrawoona Group in the eastern Pilbara Craton, western Australia, *Precambrian Res., 80*, 89-105, 1996.

Zegers, T.E., M. de Keijzer, C.W. Passchier, and S.H. White, The Mulgandinnah Shear Zone: An Archean crustal scale shear zone in the eastern Pilbara, western Australia, *Precambrian Res., 88*, 233-247, 1998.

Zegers, T.E., J.R. Wijbrans, and S.H. White, $^{40}Ar/^{39}Ar$ age constraints on tectonothermal events in the Shaw Area of the eastern Pilbara granite-greenstone terrain (W. Australia). 700 Ma of Archean tectonic evolution, *Tectonophysics, 311*, 45-81, 1999.

D. R. Nelson, Western Australian Isotope Studies Research Group, Department of Applied Physics, Curtin University of Technology, GPO Box U1987, Perth, WA, 6001, Australia. (D.Nelson@curtin.edu.au)

S. H. White and T. E. Zegers, Vening Meinesz Research School of Geodynamics, Faculty of Earth Sciences, Utrecht University, P.O. Box 80021, 3508 TA Utrecht, Netherlands. (swhite@geo.uu.nl; tanja@geo.uu.nl)

J. R. Wijbrans, Department of Isotope Geochemistry, Faculty of Earth Sciences, Vrije University, 1081 HV Amsterdam, Netherlands. (wijj@geo.vu.nl)

(Received March 15, 2000;
revised May 23, 2001;
accepted June 5, 2001.)